Conformal relativistic viscous hydrodynamics: Applications to RHIC results at $\sqrt{s_{NN}}$ = 200 GeV

Matthew Luzum[1] and Paul Romatschke[2]

[1]*Theoretical Nuclear Physics Group, Department of Physics, University of Washington, Box 351560, Seattle, Washington 98195, USA*

[2]*Institute for Nuclear Theory, University of Washington, Box 351550, Seattle, Washington 98195, USA*

(Received 20 May 2008; published 26 September 2008)

A new set of equations for relativistic viscous hydrodynamics that captures both weak-coupling and strong-coupling physics to second order in gradients has been developed recently. We apply this framework to bulk physics at the Relativistic Heavy Ion Collider (RHIC), both for standard (Glauber-type) as well as for color-glass-condensate (CGC) initial conditions and show that the results do not depend strongly on the values for the second-order transport coefficients. Results for multiplicity, radial flow and elliptic flow are presented, and we quote the ratio of viscosity over entropy density for which our hydrodynamic model is consistent with experimental data. For CGC initial conditions, early thermalization does not seem to be required in order for hydrodynamics to describe charged hadron elliptic flow.

DOI: 10.1103/PhysRevC.78.034915 PACS number(s): 12.38.Mh, 25.75.Ld, 47.75.+f

I. INTRODUCTION

The experimental program at the Relativistic Heavy Ion Collider (RHIC) at Brookhaven has generated a wealth of data [1–4] on QCD matter at the highest energy densities obtained in the laboratory. Remarkably, ideal hydrodynamics seems to offer a sensible description of the experimental data for bulk properties (multiplicity, radial and elliptic flow) of low-p_T particles for heavy-ion collisions at RHIC [5–9].

Upon closer inspection, however, not all of this success can be attributed to modeling the system as an ideal fluid. For instance, the energy density distribution used as an initial condition for the hydrodynamic equations is customarily chosen such that the output from the hydrodynamic model matches the experimental data for the multiplicity. Furthermore, the time at which the hydrodynamic model is initialized and the temperature (or energy density) at which the hydrodynamic evolution is stopped are typically chosen such that the model output matches the experimental data for the radial flow. After these parameters have been fixed, only the good description of experimental data for the elliptic flow coefficient can be considered a success for ideal hydrodynamics (in the sense that it is parameter free).

To make progress and learn more about the properties of matter created at RHIC, the task is now to both test and improve this ideal hydrodynamic model. The obvious framework for this task is dissipative hydrodynamics, since it contains ideal hydrodynamics as the special case when all dissipative transport coefficients (such as shear and bulk viscosity and heat conductivity) are sent to zero. If the values of the transport coefficients were known (e.g., by some first principle calculation), then one could use dissipative hydrodynamics to constrain, e.g., the initial energy density distribution, which is chosen conveniently in the ideal hydrodynamic models. Or otherwise, choosing again physically acceptable initial conditions, one is able to constrain the allowed ranges of the transport coefficients. Despite recent progress in first principle calculations [10–19], the values of the hydrodynamic transport coefficients for QCD in the relevant energy range are poorly constrained to date, so the second option is currently the only viable possibility.

For RHIC, the first step in this direction was carried out by Teaney [20], who provided estimates for the sign and size of corrections due to shear viscosity. This famous calculation, however, did not provide a description of experimental data for nonzero viscosity, because it was not dynamic and the initial conditions could not be altered. Only very recently, the first hydrodynamic calculations with shear viscosity describing particle spectra for central and noncentral collisions at RHIC have become available [21–23].

Several other groups have produced numerical codes capable of performing similar matching to data [24–31].

However, the precise formulation of the viscous hydrodynamic equations themselves has long been debated. To appreciate the complication, one first has to understand that a hydrodynamic formulation for RHIC physics necessarily has to be fully relativistic, and that the relativistic generalization of the Navier-Stokes equations are acausal since they contain modes that transport information at superluminal speeds. These are high wave number modes and therefore in principle are outside the range of validity of hydrodynamics, but in practice, one has to find a way to deal with them in viscous hydrodynamic simulations. A possible solution to this problem is known as the Müller-Israel-Stewart theory, where for each transport coefficient, a corresponding relaxation time is introduced which controls the speed of signal propagation for the high wave number modes [32–35]. For low-momentum modes (up to first order in gradients), the Müller-Israel-Stewart theory is identical to the Navier-Stokes equations, but differs for higher order gradients. Unfortunately, this implied that the resulting equations retained a certain degree of arbitrariness, as it was not clear which additional terms of second or higher order in gradients either within the Müller-Israel-Stewart or other frameworks (see, e.g., Refs. [36–39]) were allowed. For the case of nonvanishing shear viscosity only, it was shown recently [40] that the most general form implies five independent terms of second order in gradients. This form is general enough to describe the hydrodynamic

 ©2008 The American Physical Society

properties of (conformal) plasmas for both weakly coupled systems describable by the Boltzmann equation as well as infinitely strongly coupled plasmas, which are accessible via Maldacena's conjecture [41].

The aim of this work is to now apply this new set of equations for relativistic shear viscous hydrodynamics to the problem of heavy-ion collisions at RHIC. In Sec. II, we review the setup of conformal relativistic viscous hydrodynamics and our numerics for the simulation of heavy-ion collisions. In Sec. III, details about the two main models of initial conditions for hydrodynamics are given. Section IV contains our results for the multiplicity, radial flow, and elliptic flow in Au+Au collisions at top RHIC energies, as well as a note on the notion of "early thermalization." We conclude in Sec. V.

II. SETUP

The energy-momentum tensor for relativistic hydrodynamics in the presence of shear viscosity can be written as

$$T^{\mu\nu} = \epsilon u^\mu u^\nu - p\Delta^{\mu\nu} + \Pi^{\mu\nu}, \tag{1}$$

where ϵ and p are the energy density and pressure, related by an equation of state $p = p(\epsilon)$. u^μ is the fluid four-velocity which fulfills $g_{\mu\nu}u^\mu u^\nu = 1$, where the signature of the metric is $g_{\mu\nu} = (+,-,-,-)$. The projector $\Delta^{\mu\nu} = g^{\mu\nu} - u^\mu u^\nu$ is orthogonal to the fluid velocity $u_\mu \Delta^{\mu\nu} = 0$. $\Pi^{\mu\nu}$ is the viscous shear tensor which is symmetric, traceless ($\Pi^\mu_\mu = 0$), and orthogonal to the fluid velocity. Hydrodynamics describes the evolution of the energy density and fluid velocity. The evolution equations are simply given by the conservation of the energy momentum tensor $D_\mu T^{\mu\alpha} = 0$, where D_μ is the (geometric) covariant derivative. Projection of u_α and Δ^μ_α on $D_\mu T^{\mu\alpha} = 0$ gives

$$\begin{aligned}(\epsilon + p)Du^\mu &= \nabla^\mu p - \Delta^\mu_\alpha D_\beta \Pi^{\alpha\beta},\\ D\epsilon &= -(\epsilon + p)\nabla_\mu u^\mu + \tfrac{1}{2}\Pi^{\mu\nu}\nabla_{\langle\nu}u_{\mu\rangle},\end{aligned} \tag{2}$$

where $D \equiv u^\alpha D_\alpha$ and $\nabla^\mu \equiv \Delta^{\mu\alpha}D_\alpha$ can be thought of as comoving time and space derivatives, respectively. Note that $D_\mu = u_\mu D + \nabla_\mu$. The brackets $\langle\ \rangle$ denote the combination

$$A_{\langle\mu}B_{\nu\rangle} = \left(\Delta^\alpha_\mu\Delta^\beta_\nu + \Delta^\alpha_\nu\Delta^\beta_\mu - \tfrac{2}{3}\Delta^{\alpha\beta}\Delta_{\mu\nu}\right)A_\alpha B_\beta, \tag{3}$$

which is a projector that is symmetric, traceless, and orthogonal to the fluid velocity. For later convenience, we also introduce symmetric and antisymmetric brackets

$$\begin{aligned}A_{(\mu}B_{\nu)} &= \tfrac{1}{2}(A_\mu B_\nu + A_\nu B_\mu),\\ A_{[\mu}B_{\nu]} &= \tfrac{1}{2}(A_\mu B_\nu - A_\nu B_\mu).\end{aligned} \tag{4}$$

The equations (2) can be considered four equations for the four independent components of ϵ, u^μ. A theory of viscous hydrodynamics still has to specify the evolution or defining equations for the five independent components of the shear tensor $\Pi^{\mu\nu}$. To first order in gradients, these are given by the relativistic Navier-Stokes equations

$$\Pi^{\mu\nu} = \eta\nabla^{\langle\nu}u^{\mu\rangle}, \tag{5}$$

where η is the shear viscosity coefficient. As mentioned in the Introduction, this theory suffers from acausal signal propagation and associated numerical instabilities. To second order in gradients, the evolution equations are given by Ref. [40] (see also Ref. [42])

$$\begin{aligned}\Pi^{\mu\nu} = \eta\nabla^{\langle\mu}u^{\nu\rangle} &- \tau_\Pi\left[\Delta^\mu_\alpha\Delta^\nu_\beta D\Pi^{\alpha\beta} + \frac{4}{3}\Pi^{\mu\nu}(\nabla_\alpha u^\alpha)\right]\\ &+ \frac{\kappa}{2}[R^{\langle\mu\nu\rangle} + 2u_\alpha R^{\alpha\langle\mu\nu\rangle\beta}u_\beta]\\ &- \frac{\lambda_1}{2\eta^2}\Pi^{\langle\mu}{}_\lambda\Pi^{\nu\rangle\lambda} + \frac{\lambda_2}{2\eta}\Pi^{\langle\mu}{}_\lambda\omega^{\nu\rangle\lambda} - \frac{\lambda_3}{2}\omega^{\langle\mu}{}_\lambda\omega^{\nu\rangle\lambda},\end{aligned} \tag{6}$$

where $\omega_{\mu\nu} = -\nabla_{[\mu}u_{\nu]}$ is the fluid vorticity and $R^{\alpha\mu\nu\beta}$, $R^{\mu\nu}$ are the Riemann and Ricci tensors, respectively. The coefficients $\tau_\Pi, \kappa, \lambda_1, \lambda_2, \lambda_3$ are the five new coefficients controlling the size of the allowed terms of second order in gradients. Having in mind an application to the problem of heavy-ion collisions, the above set of equations can be simplified: for all practical purposes, space-time can be considered flat, such that both the Riemann and Ricci tensors vanish identically. Thus, only the four coefficients $\tau_\Pi, \lambda_1, \lambda_2, \lambda_3$ enter the problem.

A. A note on bulk viscosity and conformality

Besides shear viscosity, QCD also has nonvanishing bulk viscosity ζ which can be related to the QCD trace anomaly [43]

$$\zeta \sim T^\mu_\mu = \epsilon - 3p. \tag{7}$$

QCD lattice simulations seem to indicate that the ratio bulk viscosity over entropy density s, ζ/s, is small compared to η/s except for a small region around the QCD deconfinement transition temperature, where it is sharply peaked [44–46]. If we are interested in describing effects from shear viscosity only, we are led to consider $\zeta = 0$, or conformal fluids. This has been the main guiding principle in Ref. [40], and as a consequence Eq. (6) obeys conformal invariance, unlike most other second-order theories.[1]

B. First steps: 0+1 dimensions

To get a crude estimate of the effect of viscous corrections, let us consider the arguably simplest model of a heavy-ion collision: a system expanding in a boost-invariant fashion along the longitudinal direction and having uniform energy density in the transverse plane. Introducing the Milne variables of proper time $\tau = \sqrt{t^2 - z^2}$ and space-time rapidity $\xi = \operatorname{arctanh}(z/t)$, boost invariance simply translates to requiring all hydrodynamic variables ($\epsilon, u^\mu, \Pi^{\mu\nu}$) to be independent of rapidity, and tensor components $u^\xi, \Pi^{\mu\xi}$ to vanish. Assuming uniformity in the transverse plane furthermore requires independence from the transverse coordinates $\mathbf{x}_T = (x, y)$. Even though this means that all the velocity components except u^τ are zero, the system is nevertheless nontrivial in the sense that the sum over velocity gradients does not vanish, $\nabla_\mu u^\mu = \frac{1}{\tau}$, sometimes referred to as "Bjorken flow."

[1] Note that Muronga derived a version of Eq. (6) in Ref. [36] that turns out to obey conformal symmetry.

In a way, one has modeled an expanding system in static space-time by a system at rest in an expanding space-time. This has been achieved by transforming to the Milne coordinates τ, ξ, where the metric is $g_{\mu\nu} = \mathrm{diag}(g_{\tau\tau}, g_{xx}, g_{yy}, g_{\xi\xi}) = (1, -1, -1, -\tau^2)$. Note that even though the space-time in these coordinates is expanding, it is nevertheless flat (e.g., has vanishing Riemann tensor).

In this 0+1-dimensional toy model, the viscous hydrodynamic equations become exceptionally simple [40],

$$\begin{aligned} \partial_\tau \epsilon &= -\frac{\epsilon + p}{\tau} + \frac{\Pi^\xi_\xi}{\tau}, \\ \partial_\tau \Pi^\xi_\xi &= -\frac{\Pi^\xi_\xi}{\tau_\Pi} + \frac{4\eta}{3\tau_\Pi \tau} - \frac{4}{3\tau}\Pi^\xi_\xi - \frac{\lambda_1}{2\tau_\Pi \eta^2}\left(\Pi^\xi_\xi\right)^2. \end{aligned} \tag{8}$$

The Navier-Stokes equations are recovered formally in the limit where all second-order coefficients vanish (e.g., $\tau_\Pi, \lambda_1 \to 0$); then, one simply has

$$\Pi^\xi_\xi = \frac{4\eta}{3\tau}. \tag{9}$$

Equation (8) can be solved numerically along the lines of Refs. [38,47]. At very early times, where $\Pi^\xi_\xi > (\epsilon + p)$, the Navier-Stokes equations indicate an increase in energy density and a negative effective longitudinal pressure $p - \Pi^\xi_\xi$. Since gradients $\nabla_\mu u^\mu = 1/\tau$ are strongest at early times, this suggests that one is applying the Navier-Stokes equations outside their regime of validity. Theories including second-order gradients may be better behaved at early times, but eventually they also have to break down when gradients become too strong. Here we want to study the effects of the second-order coefficients on the value of the shear tensor at late times, where a hydrodynamic approach should be valid.

To this end, let us study the deviation of the shear tensor from its first-order value, $\delta\Pi = \Pi^\xi_\xi - \frac{4\eta}{3\tau}$. At late times, Eq. (8) implies $\epsilon \sim \tau^{-4/3}$, so $\eta \sim \tau^{-1}$. Thus, if $\delta\Pi$ is small compared to the first-order value, from Eq. (8) we find

$$\delta\Pi = \frac{4\eta}{3\tau}\left(\frac{2\tau_\Pi}{3\tau} - \frac{2\lambda_1}{3\tau\eta}\right). \tag{10}$$

For a strongly coupled $\mathcal{N} = 4$ plasma [10,40,42,48], one has[2]

$$\frac{\eta}{s} = \frac{1}{4\pi}, \quad \tau_\Pi = \frac{2 - \ln 2}{2\pi T}, \quad \lambda_1 = \frac{\eta}{2\pi T}, \tag{11}$$

and thus Π^ξ_ξ is larger than its first-order value by a factor of $1 + \frac{1-\ln 2}{3\pi T\tau}$. For RHIC, $T\tau \gtrsim 1$ is a reasonable estimate, so one finds that the second-order corrections to Π^ξ_ξ increase its value by a few percent over the first-order result.

As an example of the importance of obeying conformal invariance, imagine dropping the term involving $\nabla_\alpha u^\alpha$ in the first line of Eq. (6). Redoing the above calculation one finds

$$\delta\Pi_{\mathrm{NC}} = \frac{4\eta}{3\tau}\left(\frac{2\tau_\Pi}{\tau} - \frac{2\lambda_1}{3\tau\eta}\right), \tag{12}$$

which indicates a nearly ten-fold increase of the size of $\delta\Pi$ for the nonconformal theory. For a weakly coupled plasma well described by the Boltzmann equation [40], where one has $\tau_\Pi = \frac{6\eta}{sT}$ (λ_1 is unknown but generally set to zero in Müller-Israel-Stewart theory), the effect may be less pronounced, but still one qualitatively expects second-order effects to be anomalously large if conformal invariance is broken in an ad hoc manner.

Clearly, the above estimates are not meant to be quantitative. Indeed, even the sign of the correction may change when allowing more complicated (e.g., three-dimensional) dynamics. However, the lesson to be learned from this exercise is that second-order gradients can and indeed do modify the shear tensor from its first-order (Navier-Stokes) value. This is physically acceptable, as long as the second-order corrections are small compared to the first-order ones (otherwise the system is probably too far from equilibrium for even a hydrodynamic description correct to second order in gradients to be valid). A practical means for testing this is calculating physical observables for different values of the second-order coefficients and making sure that the results do not strongly depend on the choice for these specific values.

C. Including radial flow: Lessons from 1+1 dimensions

Some more insight into the effect of viscous corrections may be gained by improving the model of the previous subsection to allow for radially symmetric dynamics in the transverse plane (but still assuming boost invariance). This is most easily implemented by changing to polar coordinates $(x, y) \to (r, \phi)$ with $r = \sqrt{x^2 + y^2}$ and $\phi = \arctan(y/x)$. In this case, the only nonvanishing velocity components are u^τ and u^r, and hence the vorticity $\omega^{\mu\nu}$ vanishes identically. Although nontrivial, the radially symmetric flow case is still a major simplification over the general form in Eq. (6), since again the terms involving $\kappa, \lambda_2, \lambda_3$ drop out.

Such a formulation allows both important code tests [49] and realistic simulations of central heavy-ion collisions [21] to be made [note that truncated versions of Eq. (6) were used in these works]. The advantage of this formulation is that since the equations are comparatively simple, it is rather straightforward to implement them numerically, and they are not very time consuming to solve, since only one-dimensional (radial) dynamics is involved. The shortcoming of simulations with radially symmetric flow profiles ("radial flow") is that by construction they cannot be matched to experimental data on the impact-parameter dependence of multiplicity. Thus, the considerable freedom in the initial/final conditions inherent to all hydrodynamic approaches cannot be eliminated in this case.

For this reason, we choose not to discuss the case of radial flow in more detail here, but rather will comment on it later as a special case of the more general situation.

D. Elliptic flow: 2+1-dimensional dynamics

Retaining the assumption of boost invariance, but allowing for general dynamics in the transverse plane, it is useful to keep Cartesian coordinates in the transverse plane, and thus

[2]For completeness, we also mention the results $\kappa = \frac{\eta}{\pi T}, \lambda_2 = -\frac{\eta \ln 2}{\pi T}, \lambda_3 = 0$ from Refs. [40,42].

u^τ, u^x, u^y are the nonvanishing fluid velocities. The main reason is that, e.g., in polar coordinates the equations for the three independent components of $\Pi^{\mu\nu}$ would involve some extra nonvanishing Christoffel symbols (other than $\Gamma^\tau_{\xi\xi} = \tau$ and $\Gamma^\xi_{\tau\xi} = 1/\tau$).

Fortunately, the case of two dimensions is special insofar as the only nontrivial component of the vorticity tensor, namely, ω^{xy}, fulfills the equation [22]

$$D\omega^{xy} + \omega^{xy}\left[\nabla_\mu u^\mu + \frac{Dp}{\epsilon + p} - \frac{Du^\tau}{u^\tau}\right] = \mathcal{O}(\Pi^3), \quad (13)$$

which can be derived by forming the combination $\nabla^x Du^y - \nabla^y Du^x$. The expression $\mathcal{O}(\Pi^3)$ denotes that the right-hand side of Eq. (13) is of third order in gradients, and thus should be suppressed in the domain of applicability of hydrodynamics. For heavy-ion collisions, typically $\nabla_\mu u^\mu \geqslant \frac{1}{\tau}$, so that for an equation of state with a speed of sound squared $c_s^2 \equiv \frac{dp(\epsilon)}{d\epsilon} \sim \frac{1}{3}$, Eq. (13) translates to $\frac{D\omega^{xy}}{\omega^{xy}} < 0$ unless $D \ln u^\tau \geqslant (1 - c_s^2)\nabla_\mu u^\mu$. In particular, this implies that in general $\omega^{xy} = 0$ is a stable fix point of the above equation, and hence we expect ω^{xy} to remain small throughout the entire viscous hydrodynamic evolution if it is small initially.

Generically, one uses $u^{x,y} = 0$ as an initial condition for hydrodynamics [50], which implies $\omega^{xy} = 0$ initially. Therefore, to very good approximation we can neglect the terms involving vorticity in Eq. (6), such that again only the second-order coefficients τ_Π, λ_1 have to be specified.

The equations to be solved for 2+1-dimensional relativistic viscous hydrodynamics are then (in components)

$$\begin{aligned}
(\epsilon + p)Du^i &= c_s^2(g^{ij}\partial_j\epsilon - u^i u^\alpha \partial_\alpha \epsilon) - \Delta^i_\alpha D_\beta \Pi^{\alpha\beta},\\
D\epsilon &= -(\epsilon + p)\nabla_\mu u^\mu + \frac{1}{2}\Pi^{\mu\nu}\nabla_{\langle\mu}u_{\nu\rangle},\\
D_\beta \Pi^{\alpha\beta} &= \Pi^{i\alpha}\partial_\tau \frac{u^i}{u^\tau} + \frac{u^i}{u^\tau}\partial_\tau \Pi^{i\alpha} + \partial_i \Pi^{\alpha i}\\
&\quad + \Gamma^\alpha_{\beta\delta}\Pi^{\beta\delta} + \Gamma^\beta_{\beta\delta}\Pi^{\alpha\delta},\\
\partial_\tau \Pi^{i\alpha} &= -\frac{4}{3u^\tau}\Pi^{i\alpha}\nabla_\beta u^\beta + \frac{\eta}{\tau_\Pi u^\tau}\nabla^{\langle i}u^{\alpha\rangle} - \frac{1}{\tau_\Pi u^\tau}\Pi^{i\alpha}\\
&\quad - \frac{u^i\Pi^\alpha_\kappa + u^\alpha \Pi^i_\kappa}{u^\tau}Du^\kappa - \frac{u^j}{u^\tau}\partial_j \Pi^{i\alpha}\\
&\quad - \frac{\lambda_1}{2\eta^2\tau_\Pi u^\tau}\Pi^{\langle i}_\lambda \Pi^{\alpha\rangle\lambda},\\
\nabla_\mu u^\mu &= \partial_\tau u^\tau + \partial_i u^i + \frac{u^\tau}{\tau},\\
\nabla_{\langle x}u_{x\rangle} &= 2\Delta^{\tau x}\partial_\tau u^x + 2\Delta^{ix}\partial_i u^x - \frac{2}{3}\Delta^{xx}\nabla_\mu u^\mu,\\
\nabla_{\langle x}u_{y\rangle} &= \Delta^{\tau x}\partial_\tau u^y + \Delta^{\tau y}\partial_\tau u^x + \Delta^{ix}\partial_i u^y\\
&\quad + \Delta^{iy}\partial_i u^x - \frac{2}{3}\Delta^{xy}\nabla_\mu u^\mu,\\
\nabla_{\langle\xi}u_{\xi\rangle} &= 2\tau^4\Delta^{\xi\xi}\Gamma^\xi_{\tau\xi}u^\tau - \frac{2}{3}\tau^4\Delta^{\xi\xi}\nabla_\mu u^\mu. \qquad (14)
\end{aligned}$$

Here and in the following discussion, Latin indices collectively denote the transverse coordinates (x, y), and the relation $u_\mu \Pi^{\mu\nu} = 0$ has been used to derive the above equations (similarly, $u^\mu \nabla_{\langle\mu}u_{\nu\rangle} = 0$ can be used to obtain the other nontrivial components needed). Note that this particular form of Eq. (14) has not been simplified further, since it roughly corresponds to the equations implemented for the numerics of Ref. [22] and is meant to facilitate understanding of the code [51]. A simple algorithm to solve Eq. (14) has been outlined in Ref. [49] and will be reviewed in the next subsection for completeness.

E. A numerical algorithm to solve relativistic viscous hydrodynamics

The first step of the algorithm consists of choosing the independent degrees of freedom. For boost-invariant 2+1-dimensional dynamics, a sensible choice for this set is, e.g., $\epsilon, u^x, u^y, \Pi^{xx}, \Pi^{xy}$, and Π^{yy}. The pressure is then obtained via the equation of state $p(\epsilon)$, and the only other nonvanishing velocity as $u^\tau = \sqrt{1 + u_x^2 + u_y^2}$. Similarly, the other nonzero components of $\Pi^{\mu\nu}$ are calculated using the equations $\Pi^\mu_\mu = 0$ and $u_\mu \Pi^{\mu\nu} = 0$.

Given the value of the set of independent components at some time $\tau = \tau_0$, the aim is then to construct an algorithm from Eq. (14) such that the new values of the set can be calculated as time progresses. Note that in Eq. (14), time derivatives of the independent component set enter only linearly. Therefore, Eq. (14) may be written as a matrix equation for the derivatives of the independent component set,

$$\begin{pmatrix} a_{00} & a_{01} & \dots & a_{05} \\ a_{10} & a_{11} & \dots & a_{15} \\ \dots & \dots & \dots & \dots \\ a_{50} & a_{51} & \dots & a_{55} \end{pmatrix} \cdot \begin{pmatrix} \partial_\tau \epsilon \\ \partial_\tau u^x \\ \dots \\ \partial_\tau \Pi^{yy} \end{pmatrix} = \begin{pmatrix} b_0 \\ b_1 \\ \dots \\ b_6 \end{pmatrix}. \quad (15)$$

Denoting the above matrix and vector as $\mathbf{A}$ and $\mathbf{b}$, respectively, a straightforward way to obtain the time derivatives is via numerical matrix inversion,

$$\begin{pmatrix} \partial_\tau \epsilon \\ \partial_\tau u^x \\ \dots \\ \partial_\tau \Pi^{yy} \end{pmatrix} = \mathbf{A}^{-1} \cdot \mathbf{b}. \quad (16)$$

Choosing a naive discretization of derivatives

$$\begin{aligned}
\partial_\tau f(\tau) &= \frac{f(\tau + \delta\tau) - f(\tau)}{\delta\tau},\\
\partial_x f(x) &= \frac{f(x + a) - f(x - a)}{2a},
\end{aligned} \quad (17)$$

which is first-order accurate in the temporal grid spacing $\delta\tau$ and second-order accurate in the spatial grid spacing a, one can then directly calculate the new values of the independent component set from Eq. (16).

Note that for ideal hydrodynamics, the algorithm Eq. (16) would fail for this naive discretization [52]. The reason is that ideal hydrodynamics is inherently unstable to high wave number fluctuations (which can be thought of as the basis for turbulence). For ideal hydrodynamics, one thus has to use a discretization which amounts to the introduction of numerical viscosity to dampen these fluctuations. Luckily,

viscous hydrodynamics does not suffer from this problem, because it has real, physical viscosity built in. For this reason, the naive discretization can be used in the algorithm Eq. (16) without encountering the same problems as in ideal hydrodynamics, as long as a finite value for the viscosity η is used.[3] While applicable to sufficiently smooth initial conditions, the above algorithm is too simple to treat strong gradients such as the propagation of shocks and should be replaced by a more involved scheme in such cases.

Since matrix inversions are computationally intensive, one can speed up the numerics by expressing $\partial_\tau \Pi^{\mu\nu}$ in terms of $\partial_\tau u^i$ and $\partial_\tau \epsilon$. Inserting these into the equations for Du^μ and $D\epsilon$, one only needs to invert a 3×3 matrix to obtain the new values of the energy density and fluid velocities. This approach has been used in Refs. [21,22,49].

F. Initial conditions and equation of state

As outlined in the Introduction, any hydrodynamic description of RHIC physics relies on the given initial energy density distributions. Two main classes of models for boost-invariant setups exist: the Glauber models and the color-glass-condensate (CGC) models.

As will be shown in the following, both model classes can give a reasonable description of the experimentally found multiplicity distribution, but they differ by their initial spatial eccentricity. A detailed discussion of the initial conditions will be given in subsequent sections.

Besides an initial condition for the energy density, one also needs to specify an initial condition for the independent components of the fluid velocities and the shear tensor. For the fluid velocities, we will follow the standard assumption that these vanish initially [50]. Finally, when using the set of equations (14), one also has to provide initial values for the independent components of $\Pi^{\mu\nu}$. Extreme choices are $\Pi^{\mu\nu} = 0$ and a shear tensor so large that a diagonal component of the energy-momentum tensor vanishes in the local rest frame (e.g., $\Pi^\xi_\xi = p$, or zero longitudinal effective pressure), with the physical result expected somewhere in between (see, e.g., the discussion in Ref. [53]).

Once the initial conditions for the independent hydrodynamic variables have been specified, one needs the equation of state to solve the hydrodynamic equations (14). Aiming for a description of deconfined nuclear matter at zero chemical potential, a semirealistic equation of state has to incorporate evidence from lattice QCD calculations [54] that the transition from hadronic to deconfined quark matter is probably an analytic crossover, not a first- or second-order phase transition, as often used in ideal hydrodynamic simulations. On the other hand, continuum extrapolations for the value of the energy density and pressure for physical quark masses are still not accessible with high precision using current lattice methods. For this reason, we will employ the equation of state by Laine and Schröder [55], which is derived from a hadron resonance gas at low temperatures, a high-order weak-coupling perturbative QCD calculation at high temperatures, and an analytic crossover regime interpolating between the high and low temperature regime, respectively. For hydrodynamics, an important quantity is the speed of sound squared extracted from the equation of state, $c_s^2 \equiv \frac{dp(\epsilon)}{d\epsilon}$. For completeness, we reproduce a plot of this quantity in Fig. 1.

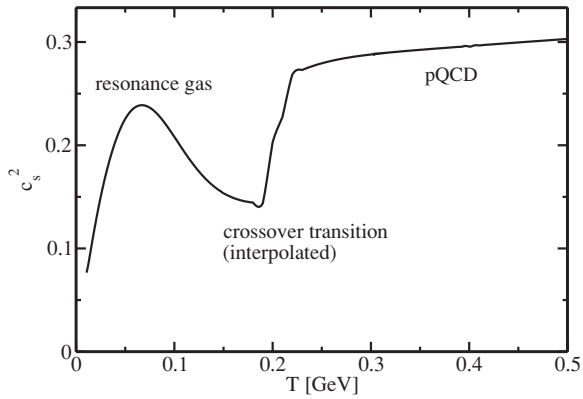

FIG. 1. Speed of sound squared from Ref. [55], used in the hydrodynamic simulations. See text for details.

G. Freeze-out

At some stage in the evolution of the matter produced in a heavy-ion collision, the system will become too dilute for a hydrodynamic description to be applicable. This "freeze-out" process most probably happens gradually, but it is difficult to model realistically. A widely used approximation is therefore to assume instantaneous freeze-out whenever a certain fluid cell cools below a certain predefined temperature or energy density (see Refs. [30,56] for different approaches). The standard prescription for this freeze-out process is the Cooper-Frye formula [57], which allows conversion of the hydrodynamic variables (energy density, fluid velocity, etc.) into particle distributions.

Specifically, in the case of isothermal freeze-out at a temperature T_f, the conversion from hydrodynamic to particle degrees of freedom will have to take place on a three-dimensional freeze-out hypersurface Σ, which can be characterized by its normal four-vector, and parametrized by three space-time variables [58,59]. The spectrum for a single particle on mass shell with four-momentum $p^\mu = (E, \mathbf{p})$ and degeneracy d is then given by

$$E\frac{d^3N}{d^3\mathbf{p}} \equiv \frac{d}{(2\pi)^3}\int p_\mu \, d\Sigma^\mu \, f\,(x^\mu, p^\mu)\,, \tag{18}$$

where $d\Sigma^\mu$ is the normal vector on the hypersurface Σ, and f is the off-equilibrium distribution function.

Originally, the Cooper-Frye prescription was derived for systems in thermal equilibrium, where f is built out of a Bose or Fermi distribution function $f_0(x) = \exp[(x) \pm 1]^{-1}$, depending on the statistics of the particle under consideration. To generalize it to systems out of equilibrium, one customarily relies on the ansatz used in the derivation of viscous

[3] In practice, we have used $\frac{\eta}{s} > 10^{-4}$. Typically, between $\frac{\eta}{s} = 10^{-2}$ and $\frac{\eta}{s} = 10^{-4}$ there are no significant changes in the hydrodynamic results, and we refer to $\frac{\eta}{s} = 10^{-4}$ as "ideal hydrodynamics."

hydrodynamics from kinetic theory [60],

$$f(x^\mu, p^\mu) = f_0\left(\frac{p_\mu u^\mu}{T}\right) + f_0\left(\frac{p_\mu u^\mu}{T}\right) \times \left[1 \mp f_0\left(\frac{p_\mu u^\mu}{T}\right)\right] \frac{p_\mu p_\nu \Pi^{\mu\nu}}{2T^2(\epsilon + p)}. \quad (19)$$

For simplicity, in the following we approximate $f_0(x) \sim \exp(-x)$, so similarly

$$f(x^\mu, p^\mu) = \exp(-p_\mu u^\mu / T)\left[1 + \frac{p_\mu p_\nu \Pi^{\mu\nu}}{2T^2(\epsilon + p)}\right]. \quad (20)$$

The effect of this approximation will be commented on in the following sections.

In practice, for boost-invariant 2+1-dimensional hydrodynamics, the freeze-out hypersurface $\Sigma^\mu = (\Sigma^t, \Sigma^x, \Sigma^y, \Sigma^z) = (t, x, y, z)$ can be parametrized either by τ, ξ and the polar angle ϕ, or by x, y, ξ:

$$\begin{aligned} t &= \tau \cosh\xi, & t &= \tau(x, y)\cosh\xi, \\ x &= x(\tau, \phi), & x &= x, \\ y &= y(\tau, \phi), & y &= y, \\ z &= \tau \sinh\xi, & z &= \tau(x, y)\sinh\xi. \end{aligned} \quad (21)$$

The normal vector on Σ^μ is calculated by

$$d\Sigma_\mu(\tau, \phi, \xi) = \varepsilon_{\mu\alpha\beta\gamma} \frac{\partial\Sigma^\alpha}{\partial\tau} \frac{\partial\Sigma^\beta}{\partial\phi} \frac{\partial\Sigma^\gamma}{\partial\xi} d\tau d\phi\, d\xi,$$

$$d\Sigma^\mu(\tau, \phi, \xi) = -\tau\left[\cosh\xi\left(\frac{\partial x}{\partial\tau}\frac{\partial y}{\partial\phi} - \frac{\partial y}{\partial\tau}\frac{\partial x}{\partial\phi}\right), \frac{\partial y}{\partial\phi}, -\frac{\partial x}{\partial\phi}, \sinh\xi\left(\frac{\partial x}{\partial\tau}\frac{\partial y}{\partial\phi} - \frac{\partial y}{\partial\tau}\frac{\partial x}{\partial\phi}\right)\right] d\tau d\phi d\xi,$$

and similarly for the other parametrization [61].

For a realistic equation of state, at early times the freeze-out hypersurface will contain the same transverse coordinate values (x, y) for different times τ (see Fig. 2). Therefore, the parametrization in terms of (x, y, ξ) cannot be used for early times. On the other hand, the parametrization in terms of (τ, ϕ, ξ) contains derivatives of (x, y) with respect to τ, which become very large at late times (see Fig. 2). Numerically, it is therefore not advisable to use this parametrization at late times. As a consequence, we use the one parametrization at early times but switch to the other parametrization at late times, such that the integral in Eq. (18) is always defined and numerically well behaved.[4]

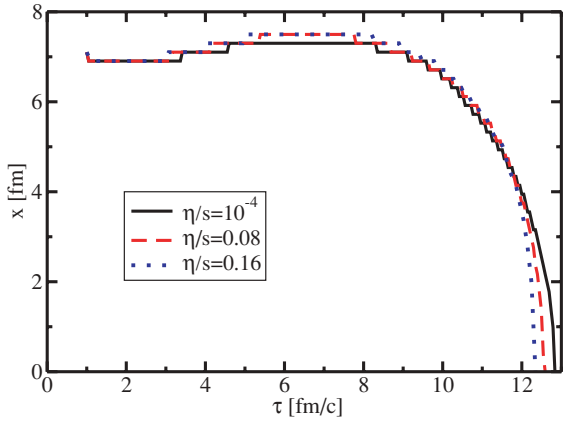

FIG. 2. (Color online) Space-time cut through the three-dimensional hypersurface for a central collision within the Glauber model. Simulation parameters used were $a = 1$ GeV^{-1}, $\tau_0 = 1$ fm/c, $T_i = 0.36$ GeV, $T_f = 0.15$ GeV, $\tau_\Pi = 6\frac{\eta}{s}$, and $\lambda_1 = 0$ (see next sections for definitions). As can be seen from the figure, inclusion of viscosity only slightly changes the form of the surface.

To evaluate the integral (18), it is useful to express p^μ also in Milne coordinates,

$$\begin{aligned} p^\mu &= (p^\tau, p^x, p^y, p^\xi) \\ &= [m_T \cosh(Y - \xi), p^x, p^y, \frac{m_T}{\tau}\sinh(Y - \xi)], \end{aligned} \quad (22)$$

where $m_T = \sqrt{m^2 + p_x^2 + p_y^2} = \sqrt{E^2 - p_z^2}$. Here and in the following, $Y = \operatorname{arctanh}(p^z/E)$ is the rapidity, and m is the rest mass of the particle under consideration. Then the ξ integration can be carried out analytically using

$$\begin{aligned} &\frac{1}{2}\int_{-\infty}^{\infty} d\xi \cosh^n(Y - \xi)\exp[-z\cosh(Y - \xi)] \\ &\quad = (-1)^n \partial_z^n K_0(z) \equiv K(n, z), \end{aligned} \quad (23)$$

where $K_0(z)$ is a modified Bessel function. One finds

$$\begin{aligned} E\frac{d^3N}{d^3\mathbf{p}} &= \frac{2d}{(2\pi)^3}\int d\tau\, d\phi \exp\frac{p^x u^x + p^y u^y}{T} \\ &\quad \times \left\{ m_T\left(\frac{\partial x}{\partial\tau}\frac{\partial y}{\partial\phi} - \frac{\partial y}{\partial\tau}\frac{\partial x}{\partial\phi}\right)\left[T_1 K\left(1, \frac{m_T u^\tau}{T}\right) + T_2 K\left(2, \frac{m_T u^\tau}{T}\right) + T_3 K\left(3, \frac{m_T u^\tau}{T}\right)\right] \right. \\ &\quad \left. - \left(p^x\frac{\partial y}{\partial\phi} - p^y\frac{\partial x}{\partial\phi}\right)\left[T_1 K\left(0, \frac{m_T u^\tau}{T}\right) + T_2 K\left(1, \frac{m_T u^\tau}{T}\right) + T_3 K\left(2, \frac{m_T u^\tau}{T}\right)\right]\right\}, \\ T_1 &= 1 + \frac{m_T^2\Pi_\xi^\xi + p_x^2\Pi^{xx} + p_y^2\Pi^{yy} + 2p_x p_y\Pi^{xy}}{2T^2(\epsilon + p)}, \\ T_2 &= -2m_T\frac{p^x\Pi^{x\tau} + p^y\Pi^{y\tau}}{2T^2(\epsilon + p)}, \\ T_3 &= m_T^2\frac{\Pi^{\tau\tau} - \Pi_\xi^\xi}{2T^2(\epsilon + p)}, \end{aligned} \quad (24)$$

for the (τ, ϕ, ξ) parametrization, and a similar result for the other parametrization of the hypersurface. The remaining integrals for the particle spectrum have to be carried out numerically unless one is considering the case of a central collision [21,49] where the integral has an additional symmetry in ϕ.

For the simulation of a heavy-ion collision, one then also needs to take into account the feed-down process of particle

[4] It may be possible that other parametrizations may turn out to be more convenient. For instance, it is conceivable that performing a triangulation of the three-dimensional hypersurface and replacing the integral in Eq. (18) by a sum over triangles could turn out to be numerically superior to our method.

resonances that decay into lighter, stable particles [62,63]. Therefore, we calculate the spectra for particle resonances with masses up to ∼2 GeV and then use available routines from the AZHYDRO package [64] to determine the spectra of stable particles including these feed-down contributions. Ultimately, one would be interested in describing the last stage of the evolution by coupling the hydrodynamics to a hadronic cascade code [65–68]. We leave this for future work.

The particle spectra $E\frac{dN_{\rm corr}}{d^3\mathbf{p}}$ including feed-down contributions can then be used to calculate experimental observables at central rapidity $Y = 0$, such as radial and elliptic flow coefficients, v_0, v_2, respectively. These are defined as

$$\begin{aligned} v_0(p_T, b) &= \int \frac{d\phi_p}{2\pi} E\frac{dN_{\rm corr}}{d^3\mathbf{p}}, \\ E\frac{dN_{\rm corr}}{d^3\mathbf{p}} &= v_0(p_T, b)[1 + 2v_2(p_T, b)\cos(2\phi_p) + \cdots], \end{aligned} \tag{25}$$

where $\phi_p = \arctan(p^y/p^x)$ and $p_T = \sqrt{p_x^2 + p_y^2}$. Furthermore, the total multiplicity per unit rapidity $\frac{dN}{dy}$ and the mean transverse momentum $\langle p_T\rangle$ are then given by

$$\begin{aligned} \frac{dN}{dy} &\equiv 2\pi \int dp_T\, p_T v_0(p_T, b), \\ \langle p_T\rangle &\equiv \frac{\int dp_T\, p_T^2 v_0(p_T, b)}{\int dp_T\, p_T v_0(p_T, b)}. \end{aligned} \tag{26}$$

The p_T integrated elliptic flow coefficient is defined as

$$v_2^{\rm int}(b) = \frac{\int dp_T\, p_T\, v_2(p_T, b) v_0(p_T, b)}{\int dp_T\, p_T v_0(p_T, b)}, \tag{27}$$

and the minimum bias elliptic flow coefficient as [7]

$$v_2^{\rm mb}(p_T) = \frac{\int db\, b\, v_2(p_T, b) v_0(p_T, b)}{\int db\, b\, v_0(p_T, b)}. \tag{28}$$

H. Code tests

It is imperative to subject the numerical implementation of the relativistic viscous hydrodynamic model to several tests. The minimal requirement is that the code be stable for a range of simulated volumes and grid spacings a, such that an extrapolation to the continuum may be attempted (keeping the simulated volume fixed but sending $a \to 0$). Our code fulfills this property.

Furthermore, one has to test whether this continuum extrapolation corresponds to the correct physical result in simple test cases. One such test case is provided by the 0+1-dimensional model discussed in Sec. II B. Using initial conditions of uniform energy density in the 2+1-dimensional numerical code, the temperature evolution should match that of Eq. (8), for which it is straightforward to write an independent numerical solver. Our 2+1-dimensional code passes this test, for small and large η/s and different values for τ_Π, λ_1.

The above test is nontrivial in the sense that it allows one to check the implementation of nonlinearities in the hydrodynamic model. However, it does not probe the dynamics of the model, since, e.g., all velocities are vanishing. Therefore, another test that one can (and should!) conduct is to study the dynamics of the model against that of linearized hydrodynamics (this test was first outlined in Ref. [49]; see Ref. [69] for similar considerations). More specifically, let us consider a viscous background "solution" with $u^i = 0$ but nonvanishing $\epsilon(\tau), \Pi_\xi^\xi(\tau)$ obeying Eq. (8). To first order in small fluctuations $\delta\epsilon, \delta u^\mu, \delta\Pi^{\mu\nu}$ around this background, the set of equations (14) becomes

$$\begin{aligned}
\left[c_s^2\partial_\tau\epsilon + \frac{1}{2}\partial_\tau\Pi_\xi^\xi + \frac{3}{2\tau}\Pi_\xi^\xi + \left(\epsilon + p + \frac{1}{2}\Pi_\xi^\xi\right)\partial_\tau\right]\delta u^x + c_s^2\partial_x\delta\epsilon + \partial_i\delta\Pi^{xi} &= 0, \\
\left[c_s^2\partial_\tau\epsilon + \frac{1}{2}\partial_\tau\Pi_\xi^\xi + \frac{3}{2\tau}\Pi_\xi^\xi + \left(\epsilon + p + \frac{1}{2}\Pi_\xi^\xi\right)\partial_\tau\right]\delta u^y + c_s^2\partial_y\delta\epsilon + \partial_i\delta\Pi^{yi} &= 0, \\
\left[\partial_\tau + \frac{1 + c_s^2}{\tau}\right]\delta\epsilon + \left[(\epsilon + p) + \frac{1}{2}\Pi_\xi^\xi\right]\partial_i\delta u^i - \frac{1}{\tau}\delta\Pi_\xi^\xi &= 0, \\
\left[\frac{4}{3\tau} + \frac{1}{\tau_\Pi} + \partial_\tau\right]\delta\Pi_\xi^\xi - \left[\frac{4\eta}{3\tau\tau_\Pi} + \frac{1}{4\tau_\Pi}\Pi_\xi^\xi\right]\frac{\delta\epsilon}{\epsilon} + \left[\frac{2\eta}{3\tau_\Pi} + \frac{4}{3}\Pi_\xi^\xi\right]\partial_i\delta u^i &= 0, \\
\left[\frac{4}{3\tau} + \frac{1}{\tau_\Pi} + \partial_\tau\right]\delta\Pi^{xx} - \left[\frac{2\eta}{3\tau_\Pi\tau} + \frac{1}{4\tau_\Pi}\Pi^{xx}\right]\frac{\delta\epsilon}{\epsilon} + \frac{2\eta}{\tau_\Pi}\partial_x\delta u^x + \left[-\frac{2\eta}{3\tau_\Pi} + \frac{4}{3}\Pi^{xx}\right]\partial_i\delta u^i &= 0, \\
\left[\frac{4}{3\tau} + \frac{1}{\tau_\Pi} + \partial_\tau\right]\delta\Pi^{xy} + \frac{\eta}{\tau_\Pi}(\partial_x\delta u^y + \partial_y\delta u^x) &= 0,
\end{aligned} \tag{29}$$

where we have put $\lambda_1 = 0$ and assumed a constant c_s^2 for simplicity. Noting that $\delta\Pi^{yy} = \delta\Pi^{\xi}_{\xi} - \delta\Pi^{xx}$ from $\delta\Pi^{\mu}_{\mu} = 0$, Eq. (29) is a closed set of linear but coupled differential equations for the fluctuations $\delta\epsilon$, δu^x, δu^y, $\delta\Pi^{\xi}_{\xi}$, $\delta\Pi^{xx}$, $\delta\Pi^{xy}$. Doing a Fourier transform,

$$\delta\epsilon(\tau, x, y) = \int \frac{d^2\mathbf{k}}{(2\pi)^2} e^{ixk^x + iyk^y} \delta\epsilon(\tau, k^x, k^y) \tag{30}$$

(and likewise for the other fluctuations), Eq. (29) comprises coupled ordinary differential equations for each mode doublet $\mathbf{k} = (k^x, k^y)$, which again are straightforward to solve with standard numerical methods [51] (and analytically for ideal hydrodynamics).

A useful test observable is the correlation function

$$f(\tau, \mathbf{x_1}, \mathbf{x_2}) = \frac{\langle \delta\epsilon(\tau, \mathbf{x_1}) \delta\epsilon(\tau, \mathbf{x_2}) \rangle}{\epsilon(\tau)^2}, \tag{31}$$

where $\langle\ \rangle$ denotes an ensemble average over initial conditions $\delta\epsilon|_{\tau=\tau_0}$. In particular, let us study initial conditions where $\delta\epsilon$ is given by Gaussian random noise with the standard deviation Δ,

$$f(\tau_0, \mathbf{x_1}, \mathbf{x_2}) = \Delta^2 \delta^2(\mathbf{x_1} - \mathbf{x_2}), \tag{32}$$

and all other fluctuations vanish initially. These initial conditions are readily implemented both for the full 2+1-dimensional hydrodynamic code and for the linearized system Eq. (29). As the system evolves to finite time τ, both approaches have to give the same correlation function f as long as the linearized treatment is applicable, and hence Eq. (29) can be used to test the dynamics of the full numerical code.

In practice, note that for the above construction f can only depend on the difference of coordinates,

$$\begin{aligned} \frac{\langle \delta\epsilon(\tau, \mathbf{x_1}) \delta\epsilon(\tau, \mathbf{x_2}) \rangle}{\epsilon(\tau)^2} &= f(\tau, \mathbf{x_1} - \mathbf{x_2}) \\ &= \int \frac{d^2\mathbf{k}}{(2\pi)^2} e^{i\mathbf{k}\cdot(\mathbf{x_1} - \mathbf{x_2})} f(\tau, \mathbf{k}), \end{aligned} \tag{33}$$

and therefore in Fourier space,

$$f(\tau, \mathbf{k}) \delta^2(\mathbf{k}') = \frac{\langle \delta\epsilon(\tau, \mathbf{k}) \delta\epsilon(\tau, \mathbf{k}' - \mathbf{k}) \rangle}{(2\pi)^2 \epsilon(\tau)^2}. \tag{34}$$

In the full 2+1-dimensional numerical code, which is discretized on a space-time lattice, $\delta^2(\mathbf{k}')$ is regular for any finite a, and one can maximize the signal for $f(\tau, \mathbf{k})$ by calculating the right-hand side of Eq. (34) for $\mathbf{k}' = 0$. Similarly, one solution $\delta\epsilon(\tau, \mathbf{k})$ per $\mathbf{k}$ mode is sufficient to calculate $f(\tau, \mathbf{k})$ for the linearized system in Eq. (29).

The above initial conditions imply $f(\tau = \tau_0, \mathbf{k}) = \Delta^2$, but for finite times characteristic peaks develop as a function of $|\mathbf{k}|$, whose position, height, and width are sensitive to the values of c_s^2, τ_Π, and η/s and of course the correct implementation of the hydrodynamic equations. The comparison between full numerics and linearized treatment shown in Fig. 3 suggests that our code also passes this test.[5]

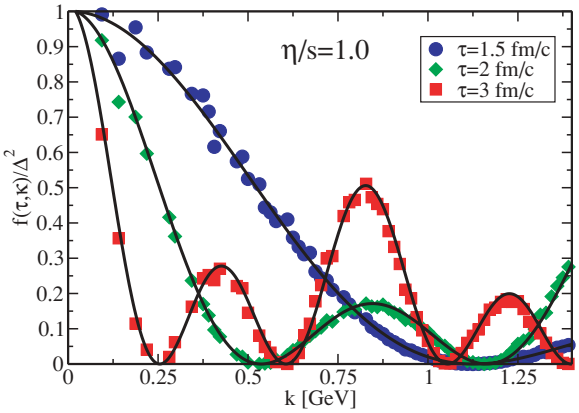

FIG. 3. (Color online) Correlation function $f(\tau, \mathbf{k})$ as a function of momentum $k = |\mathbf{k}|$ for a lattice with $a = 1$ GeV^{-1}, 64^2 sites, and averaged over 30 initial configurations (symbols), compared with the result from the linearized hydrodynamic equations (lines).

Finally, for the case of ideal hydrodynamics, analytic solutions to the hydrodynamic equations are known [70–72]. Specifically, the code for central collisions [49] has been found to agree with the results from Ref. [70] for ideal hydrodynamics. Since our code agrees with Ref. [49] for central collisions and when dropping the appropriate terms in the Eq. (6), this provides yet another test of our numerics.

To summarize, after conducting the above tests, we are reasonably confident that our numerical 2+1-dimensional code correctly solves the relativistic viscous hydrodynamic equations (14). This completes the setup of a viscous hydrodynamic description of relativistic heavy-ion collisions. In the following sections, we will review comparisons of viscous hydrodynamic simulations to experimental data, for both Glauber and CGC initial conditions.

III. INITIAL CONDITIONS: GLAUBER MODEL VS CGC

A. The Glauber model

In the Glauber model [7], the starting point is the Woods-Saxon density distribution for nuclei,

$$\rho_A(\mathbf{x}) = \frac{\rho_0}{1 + \exp\left[(|\mathbf{x}| - R_0)/\chi\right]}, \tag{35}$$

where for a gold nucleus with weight $A = 197$ we use $R_0 = 6.4$ fm and $\chi = 0.54$ fm. The parameter ρ_0 is chosen such that $\int d^3\mathbf{x} \rho_A(\mathbf{x}) = A$. One can then define the nuclear thickness function

$$T_A(x^i) = \int_{-\infty}^{\infty} dz \rho_A(\mathbf{x}), \tag{36}$$

and subsequently the number density of nucleons participating in the collision (n_{Part}) and the number density of binary

[5] Note that a small numerical error occurred in the linearized hydrodynamic solver and the corresponding figure in Ref. [22]. This error has been corrected in Fig. 3.

collisions ($n_{\rm Coll}$). For a collision of two nuclei with weight A at an impact parameter b, one has

$$\begin{aligned} n_{\rm Part}(x,y,b) &= T_A\left(x+\frac{b}{2},y\right)\\ &\quad\times\left[1-\left(1-\frac{\sigma T_A\left(x-\frac{b}{2},y\right)}{A}\right)^A\right]\\ &\quad+T_A\left(x-\frac{b}{2},y\right)\\ &\quad\times\left[1-\left(1-\frac{\sigma T_A\left(x+\frac{b}{2},y\right)}{A}\right)^A\right],\\ n_{\rm Coll}(x,y,b) &= \sigma T_A\left(x+\frac{b}{2},y\right)T_A\left(x-\frac{b}{2},y\right), \end{aligned} \tag{37}$$

where σ is the nucleon-nucleon cross section. We assume $\sigma \simeq 40$ mb for Au+Au collisions at $\sqrt{s} = 200$ GeV per nucleon pair.

While the total number of participating nucleons $N_{\rm Part}(b) = \int dxdy n_{\rm Part}(x,y,b)$ will be used to characterize the centrality class of the collision, as an initial condition for the energy density we will only use the parametrization

$$\epsilon(\tau=\tau_0,x,y,b) = \text{const}\times n_{\rm Coll}(x,y,b), \tag{38}$$

since it gives a sensible description of the multiplicity distribution of experimental data, as will be discussed later. In the following, "Glauber-model initial condition" is used synonymously with Eq. (38).

The constant in Eq. (38) is chosen such that the central energy density for zero impact parameter, $\epsilon(\tau=\tau_0,0,0,0)$, corresponds to a predefined temperature T_i via the equation of state. This temperature will be treated as a free parameter and is eventually fixed by matching to experimental data on the multiplicity.

B. The CGC model

The other model commonly used to obtain initial conditions for hydrodynamics is the so-called color-glass-condensate approach based on ideas of gluon saturation at high energies. In particular, we use a modified version of the Kharzeev-Levin-Nardi (KLN) k_T-factorization approach [73] introduced by Drescher *et al.* [74]. We follow exactly the procedure described in Ref. [53], and in fact we use the same numerical code, provided to us by the authors and only slightly modified to output initial conditions suitable for input into our viscous hydrodynamics program. In this model, the number density of gluons produced in a collision of two nuclei with atomic weight A is given by

$$\begin{aligned} \frac{dN_g}{d^2\mathbf{x}_T\,dY} &= \mathcal{N}\int\frac{d^2\mathbf{p}_T}{p_T^2}\int^{p_T}d^2\mathbf{k}_T\,\alpha_s(k_T)\\ &\quad\times\phi_A\left(x_1,\frac{(\mathbf{p}_T+\mathbf{k}_T)^2}{4};\mathbf{x}_T\right)\\ &\quad\times\phi_A\left(x_2,\frac{(\mathbf{p}_T-\mathbf{k}_T)^2}{4};\mathbf{x}_T\right), \end{aligned} \tag{39}$$

where $\mathbf{p}_T$ and Y are the transverse momentum and rapidity of the produced gluons, respectively. $x_{1,2} = p_T\times\exp(\pm Y)/\sqrt{s}$ is the momentum fraction of the colliding gluon ladders with $\sqrt{s}$ the center-of-mass collision energy, and $\alpha_s(k_T)$ is the strong coupling constant at momentum scale $k_T \equiv |\mathbf{k}_T|$.

The value of the normalization constant $\mathcal{N}$ is unimportant here, since as for Glauber initial conditions, we treat the overall normalization of the initial energy density distribution as a free parameter. The unintegrated gluon distribution functions are taken as

$$\phi(x,k_T^2;\mathbf{x}_T) = \frac{1}{\alpha_s(Q_s^2)}\frac{Q_s^2}{\max(Q_s^2,k_T^2)}P(\mathbf{x}_T)(1-x)^4, \tag{40}$$

where $P(\mathbf{x}_T)$ is the probability of finding at least one nucleon at transverse position $\mathbf{x}_T$, taken from the definition for $n_{\rm Part}$, that is,

$$P(\mathbf{x}_T) = 1-\left(1-\frac{\sigma T_A}{A}\right)^A, \tag{41}$$

where T_A and σ are as defined in the previous section.

The saturation scale at a given momentum fraction x and transverse coordinate $\mathbf{x}_T$ is given by

$$Q_s^2(x,\mathbf{x}_T) = 2\,\text{GeV}^2\left(\frac{T_A(\mathbf{x}_T)/P(\mathbf{x}_T)}{1.53/\text{fm}^2}\right)\left(\frac{0.01}{x}\right)^\lambda. \tag{42}$$

The growth speed is taken to be $\lambda = 0.288$.

The initial conditions for hydrodynamic evolution require that we specify the energy density in the transverse plane at some initial proper time τ_0 at which the medium has thermalized. Equation (39), on the other hand, is in principle valid at a time $\tau_s = 1/Q_s$ at which the medium is likely not yet in thermal equilibrium. To obtain the desired initial conditions, we again follow Ref. [53] and assume that the number of gluons is effectively conserved during the evolution from τ_s to τ_0, and so the number density profile is the same at both times, scaled by the one-dimensional Bjorken expansion $n(\tau_0) = \frac{\tau_s}{\tau_0}n(\tau_s)$. The energy density can then be obtained from the number density through thermodynamic relations—it is proportional to the number density to the 4/3 power. Again, we take the overall normalization as a free parameter, so the initial energy density is finally given as

$$\epsilon(\tau=\tau_0,\mathbf{x}_T,b) = \text{const}\times\left[\frac{dN_g}{d^2\mathbf{x}_T\,dY}(\mathbf{x}_T,b)\right]^{4/3}, \tag{43}$$

where the number density is given by Eq. (39) evaluated at central rapidity $Y = 0$.

As a final comment, it should be pointed out that the original version of the CGC, the McLerran-Venugopalan model [75, 76], differs from the KLN ansatz we used here, as will be discussed in the next section.

C. Spatial and momentum anisotropy

One of the key parameters discussed in the following is the eccentricity (or spatial anisotropy) of the collision geometry.

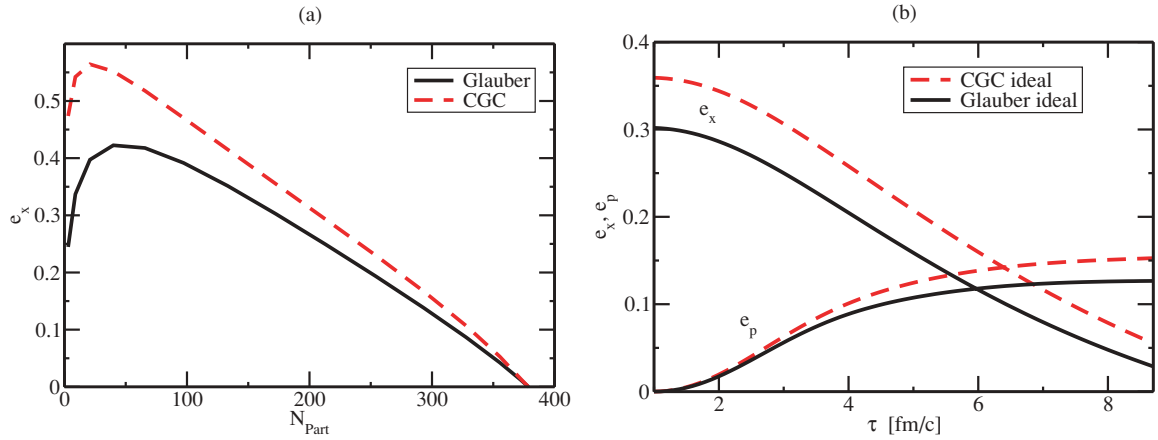

FIG. 4. (Color online) (a) Initial spatial anisotropy for the Glauber and CGC model. (b) Time evolution of the spatial and momentum anisotropy for a collision with $b = 7$ fm in ideal hydrodynamics.

Following Ref. [7], we define it as

$$e_x \equiv \frac{\langle y^2 - x^2 \rangle_\epsilon}{\langle y^2 + x^2 \rangle_\epsilon}, \tag{44}$$

where $\langle\ \rangle_\epsilon$ denotes an averaging procedure over space with the energy density ϵ as a weighting factor. Shown in Fig. 4(a), a plot of e_x for different centralities highlights the quantitative difference between the initial energy density from the Glauber and CGC models, Eq. (38) and Eq. (43), respectively. As can be seen from this figure, the CGC model generally gives a higher spatial anisotropy than the Glauber model. Note that the results for the CGC model shown here are extreme in the sense that the McLerran-Venugopalan model gives spatial eccentricities that essentially match the ones from the Glauber model [77]. This allows us to use the difference between the CGC and Glauber models as an indication of the systematic theoretical error stemming from our ignorance of the correct physical initial condition.

Hydrodynamics converts pressure gradients into fluid velocities, and hence one expects the spatial anisotropy to decrease at the expense of a momentum anisotropy (which is related to the magnitude of the elliptic flow). We follow Ref. [78] in defining a momentum anisotropy according to

$$e_p \equiv \frac{\langle T^{xx} - T^{yy} \rangle}{\langle T^{xx} + T^{yy} \rangle}, \tag{45}$$

where we stress that here $\langle\ \rangle$ denotes spatial averaging with weight factor unity. Figure 4(b) shows the time evolution in ideal hydrodynamics ($\eta/s \ll 1$) of both the spatial and momentum anisotropies for a heavy-ion collision at $b = 7$ fm modeled through Glauber and CGC initial conditions. As one can see, for the same impact parameter, the higher initial spatial anisotropy for the CGC model eventually leads to a higher momentum anisotropy than the Glauber model. Using a quasiparticle interpretation in which the energy momentum tensor is given by

$$T^{\mu\nu} \propto \int \frac{d^3\mathbf{p}}{(2\pi)^3} \frac{p^\mu p^\nu}{E} f(x^\mu, p^\mu), \tag{46}$$

the momentum anisotropy e_p can be approximately related to the integrated elliptic flow $v_2^{\text{int}}(b)$, with a proportionality factor of ~ 2 [78,79]. We find this proportionality to be maintained even for nonvanishing shear viscosity, as can be seen later in Fig. 8.

IV. RESULTS

A. Which parameters matter?

In the following, we will attempt to obtain limits on the mean value (throughout the hydrodynamic evolution) of the ratio η/s from experimental data. While, e.g., temperature variations of η/s are to be expected in the real physical systems, probing for such variations would invariably force us to introduce more unknown parameters. We prefer to leave this program for future studies once robust results for the mean value of η/s exist. Having fixed the equation of state and the freeze-out procedure as explained in the previous sections, the remaining choices that have to be made in the hydrodynamic model are the

(i) Initial energy density profile: Glauber or CGC
(ii) Initial value of shear tensor: vanishing or Navier-Stokes value
(iii) Hydrodynamic starting time τ_0
(iv) Second-order coefficients: relaxation time τ_Π and λ_1
(v) Ansatz for nonequilibrium particle distribution Eq. (19).

It is to be understood that we fix the initial energy density normalization T_i and the freeze-out temperature T_f such that the model provides a reasonable description of the experimental data on multiplicity and $\langle p_T \rangle$. Historically, a strong emphasis has been placed on requiring a small value of τ_0 for ideal hydrodynamics [80,81]. For this reason, we will discuss the dependence on τ_0 separately in Sec. IV D.

A good indicator of which parameters matter is the momentum anisotropy, since it is very sensitive to the value of η/s. From Fig. 4, one therefore immediately concludes that the choice of Glauber or CGC initial conditions is important since it has a large effect on e_p. Fortunately, most of the

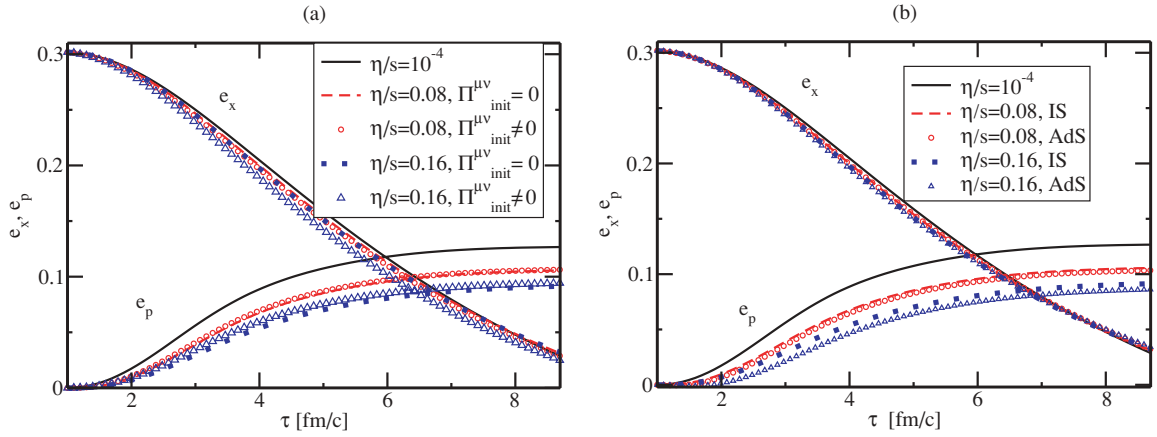

FIG. 5. (Color online) Spatial and momentum anisotropy for the Glauber model at $b = 7$ fm with $T_i = 0.353$ GeV, $\tau_0 = 1$ fm/c, and various values for the viscosity (grid spacing $a = 2$ GeV^{-1}). (a) Dependence on the initialization value of the shear tensor: shown are results for vanishing initial value ($\Pi^{\mu\nu}_{\rm init} = 0$) and Navier-Stokes initial value ($\Pi^{\mu\nu}_{\rm init} \neq 0$), given in Eq. (9). (b) Dependence on the choice of value for τ_Π, λ_1: shown are results for $\tau_\Pi = \frac{6}{T}\frac{\eta}{s}, \lambda_1 = 0$ (labeled IS), and $\tau_\Pi = \frac{2(2-\ln 2)}{T}\frac{\eta}{s}, \lambda_1 = \frac{\eta}{2\pi T}$ (labeled AdS). For $\tau_\Pi = \frac{2(2-\ln 2)}{T}\frac{\eta}{s}$, the results for $\lambda_1 = 0$ (not shown) would be visually indistinguishable from those for $\lambda_1 = \frac{\eta}{2\pi T}$.

other choices turn out to not have a strong influence on the resulting v_2 coefficient, and hence the extracted η/s. In the following we test for this sensitivity by studying e_p for a "generic" heavy-ion collision of two gold nuclei, modeled by Glauber initial conditions at an initial starting temperature of $T_i = 0.353$, an impact parameter of $b = 7$ fm, and various choices of the above parameters.

Figure 5 shows the time evolution of e_x, e_p for various values of η/s. These plots indicate that e_p (and hence v_2) clearly is sensitive to the value of η/s, suggesting that it can be a useful observable for determining the viscosity of the fluid from experiment. However, to be a useful probe of the fluid viscosity, the dependence of the final value of e_p on other parameters should be much weaker than the dependence on η/s. In Fig. 5(a), we show e_p calculated for $\Pi^{\mu\nu}(\tau_0) = 0$ and $\Pi^{\mu\nu}(\tau_0)$ equal to the Navier-Stokes value, Eq. (9). As can be seen from this figure, the resulting anisotropies are essentially independent of this choice, corroborating the finding in Refs. [29,31]. Similarly, in Fig. 5(b) we show e_p calculated in simulations where the values of the second-order transport coefficients were either those of a weakly coupled Müller-Israel-Stewart theory ($\tau_\Pi = 6\frac{\eta}{sT}, \lambda_1 = 0$) or those inspired by a strongly coupled $\mathcal{N} = 4$ SYM plasma [$\tau_\Pi = 2(2-\ln 2)\frac{\eta}{sT}, \lambda_1 = \frac{\eta}{2\pi T}$]. Again, the dependence of e_p on the choice of the values of τ_Π, λ_1 can be seen to be very weak for the values of η/s shown here. This result is in stark contrast to the findings of Ref. [29], which indicated a large sensitivity to the value of τ_Π. However, recall that Ref. [29] used evolution equations that differ from Eq. (6) and in particular do not respect conformal invariance. As argued in Sec. II B, it is therefore expected that an anomalously large sensitivity to the value of the second-order transport coefficients is to be encountered.

To study the dependence of results on the ansatz of the nonequilibrium particle distribution function (19), one would want to quantify the effect of neglecting terms of higher order in momenta in Eq. (19). To estimate this, let us rewrite $E d^3N/d^3\mathbf{p} = E\, d^3N^{(0)}/d^3\mathbf{p} + E\, d^3N^{(1)}/d^3\mathbf{p}$, where $N^{(0)}$ contains only the equilibrium part, where $f(x^\mu, p^\mu) = f_0\left(\frac{p_\mu u^\mu}{T}\right)$, and perform a Padé-type resummation,

$$E\frac{d^3N^{\rm Pade}}{d^3\mathbf{p}} \equiv E\frac{d^3N^{(0)}}{d^3\mathbf{p}}\frac{1}{1-\frac{d^3N^{(1)}}{d^3\mathbf{p}}\frac{d^3\mathbf{p}}{d^3N^{(0)}}}. \tag{47}$$

Since Eq. (47) contains powers of momenta to all orders when reexpanded, the difference between the ansatz (19) and the Padé resummed particle spectra can give insight into the systematic error of the truncation used in Eq. (19). Shown in Fig. 6, this difference suggests that this systematic error is small for momenta $p_T \lesssim 2.5$ GeV. Therefore, we do not expect our results to have a large systematic uncertainty coming from the particular ansatz (19) for these momenta.

To summarize, for values of $\eta/s \lesssim 0.2$, the results for the momentum anisotropy are essentially insensitive to the choices for the second-order transport coefficients τ_Π, λ_1 and

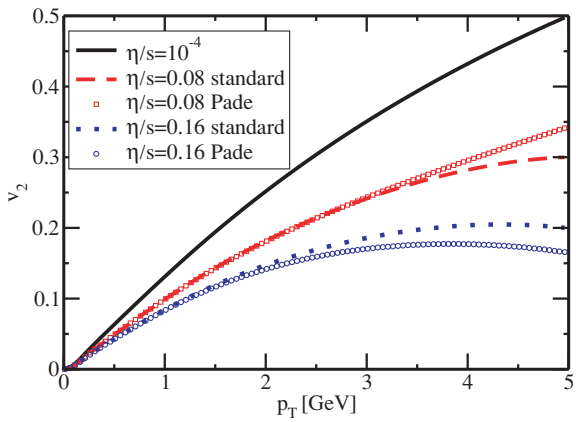

FIG. 6. (Color online) Charged hadron elliptic flow for the Glauber model at $b = 7$ fm with $T_i = 0.353$ GeV, $\tau_0 = 1$ fm/c, and various viscosities.

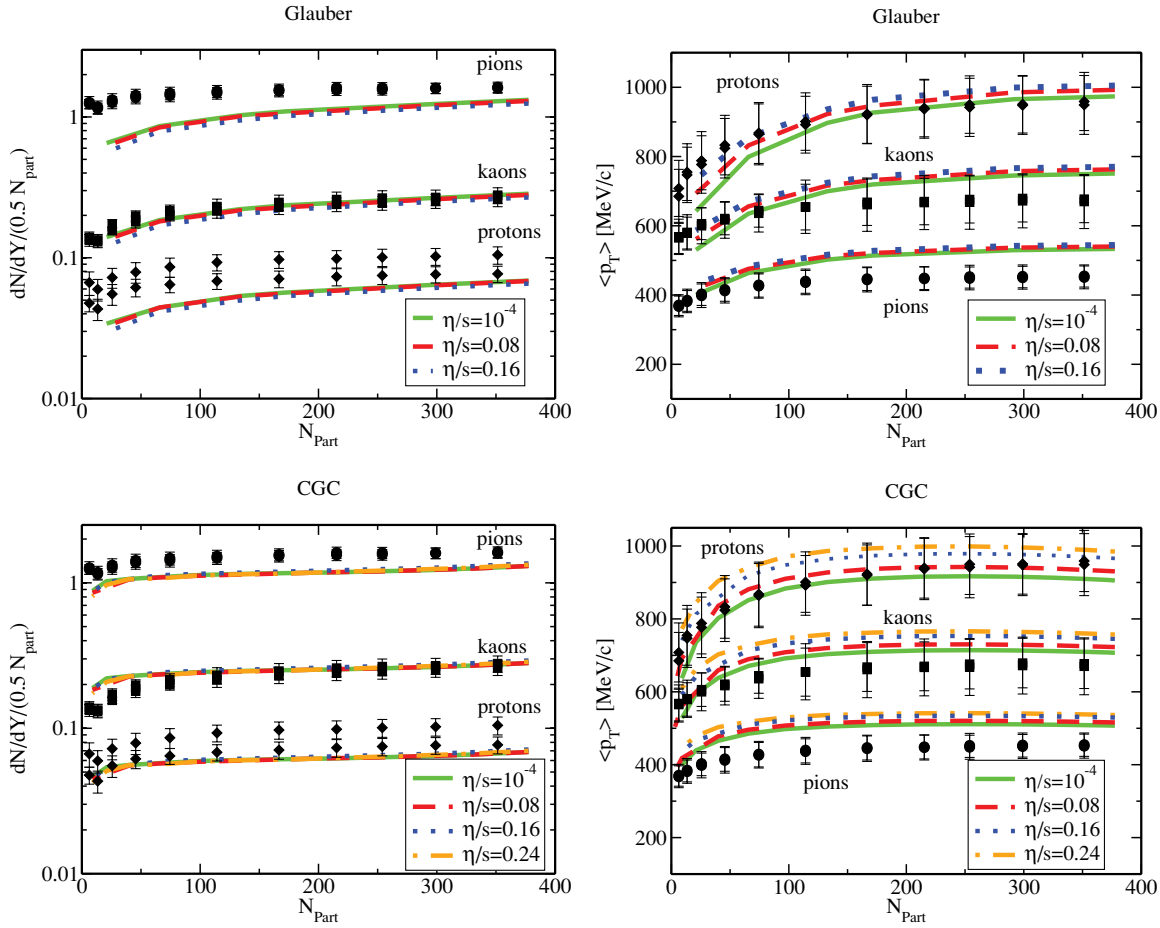

FIG. 7. (Color online) Centrality dependence of total multiplicity dN/dY and $\langle p_T \rangle$ for π^+, π^-, K^+, K^-, and p, $\bar{p}$ from PHENIX [83] for Au+Au collisions at $\sqrt{s} = 200$ GeV, compared with the viscous hydrodynamic model and various η/s, for Glauber initial conditions (from Ref. [22]) and CGC initial conditions. The model parameters used here are $\tau_0 = 1$ fm/c, $\tau_\Pi = 6\eta/s$, $\lambda_1 = 0$, $T_f = 150$ MeV, and adjusted T_i (see text for details).

the initialization of the shear tensor $\Pi^{\mu\nu}(\tau = \tau_0)$. Conversely, e_p is sensitive to the value of viscosity and the choice of initial energy density profile (initial eccentricity). Since the physical initial condition is currently unknown, this dependence will turn out to be the dominant systematic uncertainty in determining η/s from experimental data.

B. Multiplicity and radial flow

As outlined in the Introduction, we want to match the hydrodynamic model to experimental data for the multiplicity, thereby fixing the constant in Eqs. (38) and (43). This translates to fixing an initial central temperature T_i for $b = 0$, which we will quote in the following discussion.

For a constant speed of sound, the evolution for ideal hydrodynamics is isentropic, while for viscous hydrodynamics, additional entropy is produced. Since the multiplicity is a measure of the entropy of the system, one expects an increase of multiplicity for viscous compared to ideal hydrodynamic evolution. This increase in final multiplicity has been measured as a function of η/s for the semirealistic speed of sound (Fig. 1) in central heavy-ion collisions in Ref. [21], and found to be approximately[6] a factor of $0.75\eta/s$. (See Refs. [53,82] for related calculations in simplified models.) Reducing T_i accordingly therefore ensures that for viscous hydrodynamics, the multiplicity in central collisions will stay close to that of ideal hydrodynamics.

Hydrodynamics gradually converts pressure gradients into flow velocities, which in turn relate to the mean particle momenta. Starting at a predefined time τ_0 and requiring the hydrodynamic model spectra to match the experimental data on particle $\langle p_T \rangle$ then fixes the freeze-out temperature T_f.

For both Glauber-type and CGC-type model initial conditions, the experimental impact parameter dependence of the multiplicity and $\langle p_T \rangle$ is reasonably well parametrized for both ideal and viscous hydrodynamics provided T_i is adjusted accordingly (see Fig. 7). The values for T_i used in the simulations are compiled in Table I. We recall that no chemical potential is included in our equation of state, prohibiting a distinction between particles and anti-particles; and chemical and kinetic freeze-out of particles occurs at the same

[6]The quoted fraction is for a hydrodynamic starting time of $\tau_0 = 1$ fm/c. Reducing τ_0 leads to considerably larger entropy production.

TABLE I. Summary of parameters used for the viscous hydrodynamics simulations.

Initial condition	η/s	T_i (GeV)	T_f (GeV)	τ_0 (fm/c)	a (GeV^{-1})
Glauber	10^{-4}	0.36	0.15	1	1
Glauber	0.08	0.353	0.15	1	1
Glauber	0.16	0.346	0.15	1	2
CGC	10^{-4}	0.34	0.15	1	2
CGC	0.08	0.335	0.15	1	2
CGC	0.16	0.33	0.15	1	2
CGC	0.24	0.325	0.15	1	2

temperature. Furthermore, approximating the equilibrium particle distributions for bosons by a Boltzmann distribution [Eq. (19)] leads to small, but consistent underestimation of the multiplicity of light particles, such as pions. For these reasons, it does not make sense to attempt a precision fit to experimental data, especially for pions and protons. Rather, we have aimed for a sensible description of the overall centrality dependence of multiplicity and $\langle p_T \rangle$ of kaons.

Note that in particular for the CGC model, one could achieve a better fit to the data on mean $\langle p_T \rangle$ by increasing the freeze-out temperature by $\sim$10 MeV. This would also lead to a decrease in elliptic flow for this model. However, to facilitate comparison between the CGC and Glauber initial conditions, we have kept T_f the same for both models.

C. Elliptic flow

Having fixed the parameters τ_0, T_i, T_f for a given η/s to provide a reasonable description of the experimental data, a sensible comparison between the model and experimental results for the elliptic flow coefficient can be attempted. For charged hadrons, the integrated and minimum-bias v_2 coefficients are shown in Fig. 8 for Glauber and CGC initial conditions. As noted in Sec. III C, charged hadron $v_2^{\rm int}$ turns out to be very well reproduced by the momentum eccentricity $\frac{1}{2}e_p$, evaluated when the last fluid cell has cooled below T_f. This agreement is independent of impact parameter or viscosity and hence may serve as a more direct method for obtaining an estimate for $v_2^{\rm int}$ if one cannot (or does not want to) make

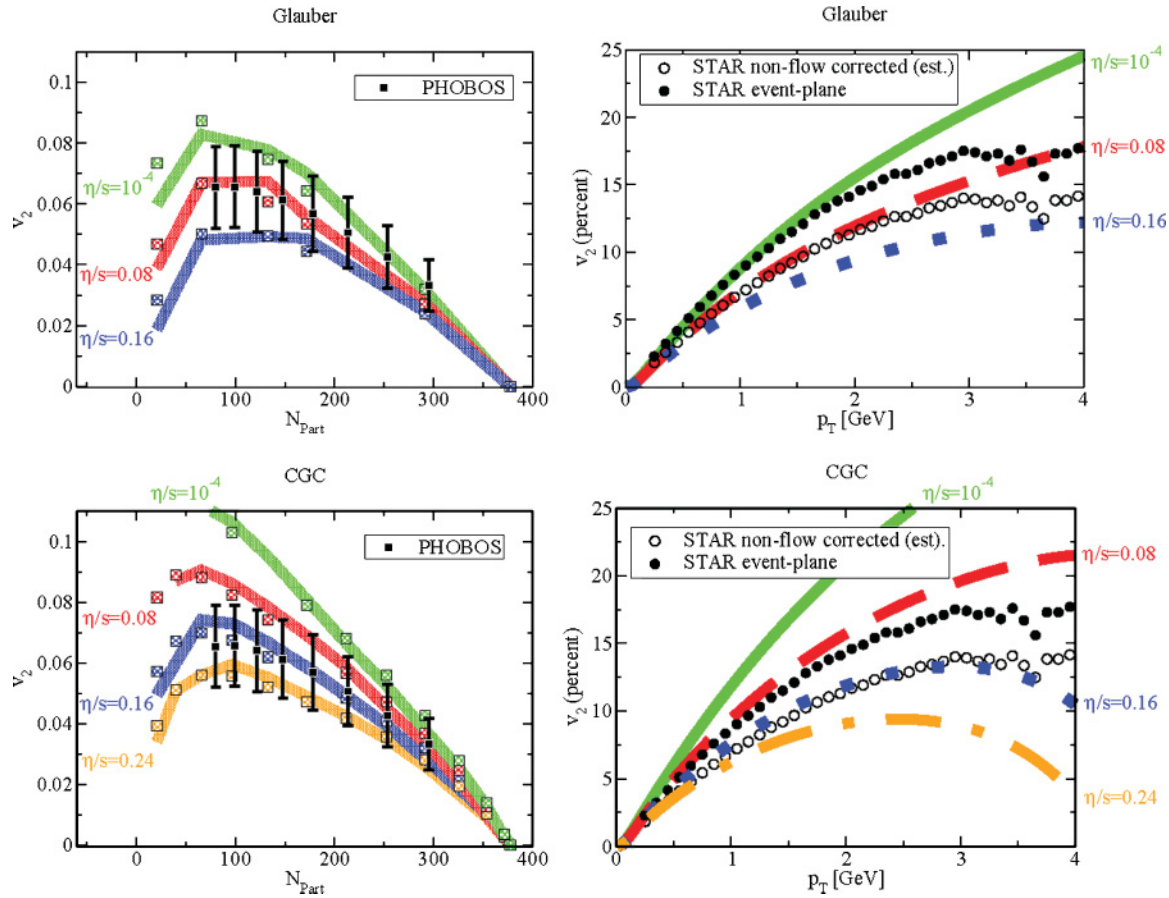

FIG. 8. (Color online) Comparison of hydrodynamic models and experimental data on charged hadron integrated (left) and minimum bias (right) elliptic flow by PHOBOS [84] and STAR [86], respectively. STAR event-plane data have been reduced by 20% to estimate the removal of nonflow contributions [86,87]. The line thickness for the hydrodynamic model curves is an estimate of the accumulated numerical error (due to, e.g., finite grid spacing). The integrated v_2 coefficient from the hydrodynamic models (full lines) is well reproduced by $\frac{1}{2}e_p$ (dots); indeed, the difference between the full lines and dots gives an estimate of the systematic uncertainty of the freeze-out prescription.

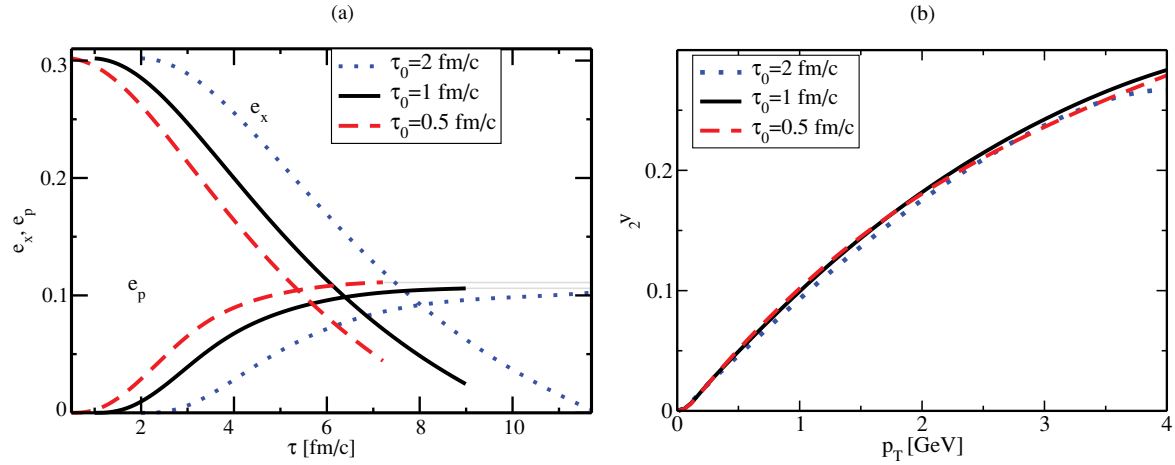

FIG. 9. (Color online) Momentum anisotropy (a) and elliptic flow for charged hadrons (b) for $b = 7$ fm, $\eta/s = 0.08$, and different hydrodynamic initialization times τ_0. Horizontal light gray lines in (a) are visual aids to compare the final value of e_p. As can be seen from these plots, neither the final e_p nor the charged hadron v_2 depend sensitively on the value of τ_0 if the same energy distribution is used as initial condition at the respective initialization times. Simulation parameters were $T_i = 0.29$ GeV, $T_f = 0.14$ GeV for $\tau_0 = 2$ fm/c; $T_i = 0.36$ GeV, $T_f = 0.15$ GeV for $\tau_0 = 1$ fm/c; and $T_i = 0.43$ GeV, $T_f = 0.16$ GeV for $\tau_0 = 0.5$ fm/c.

use of the Cooper-Frye freeze-out procedure described in Sec. II G.

The comparison of the hydrodynamic model to experimental data with 90% confidence level systematic error bars from PHOBOS [84] for the integrated elliptic flow in Fig. 8 suggests a maximum value of $\eta/s \sim 0.16$ for Glauber-type and $\eta/s \sim 0.24$ for CGC-type initial conditions. Whereas for Glauber initial conditions, ideal hydrodynamics ($\eta/s \sim 0$) gives results consistent with PHOBOS data; for CGC initial conditions, zero viscosity does not give a good fit to the data, which is consistent with previous findings [67].

For minimum-bias v_2, to date only experimental data using the event-plane method are available, where the statistical, but not the systematic, error of that measurement is directly accessible. The dominant source of systematic error is associated with the presence of so-called nonflow effects [85]. Recent results from STAR suggest that removal of these nonflow effects imply a reduction of the event-plane minimum bias v_2 by 20% [86,87]. For charged hadrons, a comparison of both the event-plane and the estimated nonflow corrected experimental data from STAR with the hydrodynamic model is shown in Fig. 8.

For Glauber-type initial conditions, the data on minimum-bias v_2 for charged hadrons is consistent with the hydrodynamic model for viscosities in the range $\eta/s \in [0, 0.1]$, while for the CGC case, the respective range is $\eta/s \in [0.08, 0.2]$. It is interesting to note that for Glauber-type initial conditions, experimental data for both the integrated and the minimum-bias elliptic flow coefficient (corrected for nonflow effects) seem to be reproduced best[7] by a hydrodynamic model with $\eta/s = 0.08 \simeq \frac{1}{4\pi}$. This number first appeared in the gauge/string duality context [10] and has been conjectured to be the universal lower bound on η/s for any quantum field theory at finite temperature and zero chemical potential [88]. For CGC-type initial conditions, the charged hadron v_2 data seem to favor a hydrodynamic model with $\eta/s \sim 0.16$, well above this bound.

D. Early vs late thermalization

Currently, there seems to be a common misunderstanding in the heavy-ion community that hydrodynamic models can universally only reproduce experimental data if they are initialized at early times $\tau_0 < 1$ fm/c. This notion has been labeled "early thermalization" and continues to create a lot of confusion. In this section, we argue that the matching of hydrodynamics to data itself does not require $\tau_0 < 1$ fm/c. It is the additional assumptions about preequilibrium dynamics that lead to this conclusion for the Glauber initial conditions.

Performing hydrodynamic simulations in the way we described earlier, the energy density distribution is specified by either the Glauber or CGC model at an initial time τ_0. In Fig. 9, we show the result for the elliptic flow coefficient (or the momentum anisotropy) for three different values of τ_0, namely, 0.5, 1, and 2 fm/c, where also T_i and T_f have been changed to obtain roughly the same multiplicity and mean p_T for each τ_0. As can be seen from this figure, the resulting final elliptic flow coefficient is essentially independent of the choice of τ_0. In particular, this implies that experimental data for bulk quantities can be reproduced by hydrodynamic models also for large initialization times, so no early thermalization assumption is needed.

However, it is true that the above procedure assumes that the energy density distribution remains unchanged up to the starting time of hydrodynamics, which arguably becomes increasingly inaccurate for larger τ_0. It has therefore been

[7]In Ref. [22], a lower value of η/s for the Glauber model was reported. The results for viscous hydrodynamics shown in Fig. 8 are identical to those in Ref. [22], but the new STAR data with nonflow corrections became available only after Ref. [22] had been published.

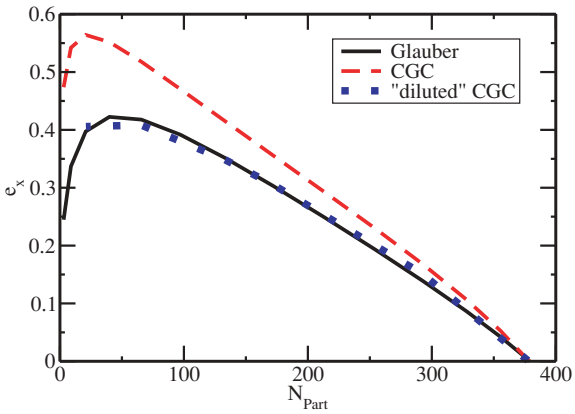

FIG. 10. (Color online) Spatial eccentricity for the Glauber and CGC models compared with evolving the CGC model according to Eq. (48) for $\tau = 1.5$ fm/c. This implies that starting with Glauber-type initial conditions at $\tau_0 > 1$ fm/c may not be unreasonable.

suggested [80] that the prehydrodynamic time evolution of the energy density distribution be mimicked by assuming free-streaming of partons. Assuming free-streaming gives the maximal contrast to assuming hydrodynamic evolution, since the latter corresponds to very strong interactions, while the former corresponds to no parton interactions at all. Indeed, one can calculate the effect of the free-streaming evolution on the spatial anisotropy, finding [80]

$$e_x(\tau) = \frac{e_x(0)}{1 + \frac{\tau^2}{3\langle R^2\rangle}}, \quad \langle R^2\rangle = \frac{\int d^2\mathbf{x}\epsilon(\tau = 0)}{\int d^2\mathbf{x}\frac{(x^2+y^2)}{2}\epsilon(\tau = 0)}. \quad (48)$$

This implies that the spatial anisotropy decreases with time, whereas one can show that free-streaming does not lead to a buildup of e_p. In other words, the eccentricity gets diluted without producing elliptic flow, such that once hydrodynamic evolution starts, it will not lead to as much v_2 as it would have without the dilution effect.[8] It is tempting to conclude from this that by comparing to experimental data on elliptic flow one could place an upper bound on the maximally allowed dilution time, and interpret this as the thermalization time of the system. One should be aware, however, that this bound will depend on the assumption made about the prehydrodynamic evolution. Furthermore, one should take into account the fact that the initial state of the system remains unknown. For instance, the system could start with an energy density distribution similar to the CGC model, which has a fairly large eccentricity. Figure 10 shows that when allowing the eccentricity to get diluted according to Eq. (48), it takes a time of $\tau \sim 1.5$ fm/c until the eccentricity has shrunk to that of the Glauber model. This implies that even when assuming no particle interactions (no elliptic flow buildup) for the first stage of the system evolution, one can get eccentricities that are Glauber-like after waiting for a significant fraction of the system lifetime. Allowing at least some particle interactions (which is probably more realistic), one expects some buildup of elliptic flow already in the dilution (or preequilibrium) phase, and therefore dilution (or "thermalization") times of $\tau \sim 2$ fm/c seem to be compatible with the observed final elliptic flow even for nonvanishing viscosity.

[8]It seems that if one forces the energy-momentum tensor at the end of the free-streaming period to match that of *ideal* hydrodynamics (instantaneous thermalization), the resulting fluid velocities are anisotropic, i.e., they correspond to a nonvanishing elliptic flow coefficient [89,90]. It is possible that this effect stems from neglecting velocity gradients (viscous hydrodynamic corrections) in the matching process. We ignore the complications of the detailed matching from free-streaming to hydrodynamics in the following.

V. SUMMARY AND CONCLUSIONS

In this article, we applied conformal relativistic viscous hydrodynamics to simulate Au+Au collisions at RHIC at energies of $\sqrt{s} = 200$ GeV per nucleon pair. Besides one first-order transport coefficient (the shear viscosity), in general there are five second-order transport coefficients in this theory, for which one would have to supply values. We provided arguments that physical observables in the parameter range accessible to hydrodynamics (low momenta, central to semicentral collisions) do not seem to be strongly dependent on specific (reasonable) choices for any of these second-order coefficients. On the other hand, we do find a pronounced dependence of the elliptic flow coefficient on the ratio of shear viscosity over entropy density, which suggests that by combining viscous hydrodynamics and experimental data, a measurement of the quark-gluon plasma viscosity may not be futile. However, we have shown that our ignorance about the precise distribution of energy density at the earliest stages of a heavy-ion collision introduces a large systematic uncertainty in the final elliptic flow of the hydrodynamic model. Adding to this is the considerable experimental uncertainty pertaining to the removal of nonflow contributions to the elliptic flow. For these reasons, we are unable to make precise statements about the value of the shear viscosity of the quark-gluon plasma and in particular cannot place a firm lower bound on η/s. Indeed, our hydrodynamic models seem to be able to consistently describe experimental data for multiplicity, radial flow, and elliptic flow of bulk charged hadrons for a wide range of viscosity over entropy ratios,

$$\frac{\eta}{s} = 0.1 \pm 0.1(\text{theory}) \pm 0.08(\text{experiment}), \quad (49)$$

where we estimated the systematic uncertainties for both theory and experiment from the results shown in Fig. 8. We stress that Eq. (49) does not account for physics not included in our model, such as finite chemical potential, bulk viscosity, heat flow, hadron cascades, three-dimensional fluid dynamic effects, and possibly many more. Consistent inclusion of all these may result in changes of the central value and theory uncertainty in Eq. (49). Nevertheless, none of the mentioned refinements is currently expected to dramatically increase the elliptic flow coefficient (though some increase may be expected when, e.g., implementing partial chemical equilibrium [91]). Therefore, we seem to be able to exclude viscosities of $\eta/s \gtrsim 0.5$ with high confidence, which indicates that the quark-gluon plasma displays less friction than any other known laboratory fluid [88,92]. Other groups have come to similar conclusions [93–95].

To better quantify the shear viscosity of the quark-gluon plasma at RHIC calls for more work, both in theory and experiment. On the theory side, a promising route seems to be the study of fluctuations and comparison with existing experimental data [84,93,96–101]. For instance, it might be interesting to investigate the critical value of η/s for the onset of turbulence in heavy-ion collisions and explore possible consequences of fully developed turbulence [102]. However, maybe most importantly, a more thorough understanding of the earliest stages of a heavy-ion collision, in particular thermalization, could fix the initial conditions for hydrodynamics and hence dramatically reduce the theoretical uncertainty in final observables.

Leaving these ideas for future work, we stress that with the advent of conformal relativistic viscous hydrodynamics, at least the uncertainties of the hydrodynamic evolution itself now seem to be under control. We hope that this serves as another step toward a better understanding of the dynamics of relativistic heavy-ion collisions.

ACKNOWLEDGMENTS

We thank B. Alver, H.-J. Drescher, A. Dumitru, U. Heinz, P. Huovinen, T. Lappi, Y. Nara, A. Poskanzer, M. Rangamani, K. Rajagopal, D.T. Son, H. Song, M. Strickland, D. Teaney, and L. Yaffe for fruitful discussions. Furthermore, we would like to thank H.-J. Drescher, A. Dumitru, and Y. Nara for providing their numerical code for the CGC initial conditions; M. Laine and Y. Schröder for providing their tabulated equation of state and permission to reproduce their result in Fig. 1; and A. Poskanzer for providing tabulated experimental data from the STAR Collaboration. The work of M.L. and P.R. was supported by the U.S. Department of Energy, Grant Nos. DE-FG02-97ER41014 and DE-FG02-00ER41132, respectively.

[1] K. Adcox *et al*. (PHENIX Collaboration), Nucl. Phys. **A757**, 184 (2005).
[2] B. B. Back *et al*., Nucl. Phys. **A757**, 28 (2005).
[3] I. Arsene *et al*. (BRAHMS Collaboration), Nucl. Phys. **A757**, 1 (2005).
[4] J. Adams *et al*. (STAR Collaboration), Nucl. Phys. **A757**, 102 (2005).
[5] D. Teaney, J. Lauret, and E. V. Shuryak, Phys. Rev. Lett. **86**, 4783 (2001).
[6] P. Huovinen, P. F. Kolb, U. W. Heinz, P. V. Ruuskanen, and S. A. Voloshin, Phys. Lett. **B503**, 58 (2001).
[7] P. F. Kolb, U. W. Heinz, P. Huovinen, K. J. Eskola, and K. Tuominen, Nucl. Phys. **A696**, 197 (2001).
[8] T. Hirano and K. Tsuda, Phys. Rev. C **66**, 054905 (2002).
[9] P. F. Kolb and R. Rapp, Phys. Rev. C **67**, 044903 (2003).
[10] G. Policastro, D. T. Son, and A. O. Starinets, Phys. Rev. Lett. **87**, 081601 (2001).
[11] P. Arnold, G. D. Moore, and L. G. Yaffe, J. High Energy Phys. 05 (2003) 051.
[12] A. Nakamura and S. Sakai, Phys. Rev. Lett. **94**, 072305 (2005).
[13] P. Arnold, C. Dogan, and G. D. Moore, Phys. Rev. D **74**, 085021 (2006).
[14] S. C. Huot, S. Jeon, and G. D. Moore, Phys. Rev. Lett. **98**, 172303 (2007).
[15] J. S. Gagnon and S. Jeon, Phys. Rev. D **75**, 025014 (2007); **76**, 089902(E) (2007).
[16] G. Aarts, C. Allton, J. Foley, S. Hands, and S. Kim, Phys. Rev. Lett. **99**, 022002 (2007).
[17] H. B. Meyer, Phys. Rev. D **76**, 101701(R) (2007).
[18] A. Buchel, Phys. Lett. **B663**, 286 (2008).
[19] S. Caron-Huot and G. D. Moore, Phys. Rev. Lett. **100**, 052301 (2008).
[20] D. Teaney, Phys. Rev. C **68**, 034913 (2003).
[21] P. Romatschke, Eur. Phys. J. C **52**, 203 (2007).
[22] P. Romatschke and U. Romatschke, Phys. Rev. Lett. **99**, 172301 (2007).
[23] A. K. Chaudhuri, arXiv:0708.1252 [nucl-th].
[24] A. Muronga and D. H. Rischke, arXiv:nucl-th/0407114.
[25] A. K. Chaudhuri and U. W. Heinz, J. Phys. Conf. Ser. **50**, 251 (2006).
[26] A. Muronga, J. Phys. G **31** S1035 (2005).
[27] A. K. Chaudhuri, Phys. Rev. C **74**, 044904 (2006).
[28] Ph. Mota, G. S. Denicol, T. Koide, and T. Kodama, J. Phys. G **34**, S1011 (2007).
[29] H. Song and U. W. Heinz, Phys. Lett. **B658**, 279 (2008).
[30] K. Dusling and D. Teaney, Phys. Rev. C **77**, 034905 (2008).
[31] Huichao Song and Ulrich Heinz, Phys. Rev. C **77**, 064901 (2008).
[32] W. Israel, Ann. Phys. (NY) **100**, 310 (1976).
[33] W. Israel and J. M. Stewart, Phys. Lett. **A58**, 213 (1976).
[34] W. Israel and J. M. Stewart, Ann. Phys. (NY) **118**, 341 (1979).
[35] I.-Shih Liu, I. Müller, and T. Ruggeri, Ann. Phys. (NY) **169**, 191 (1986).
[36] A. Muronga, Phys. Rev. C **69**, 034903 (2004).
[37] U. W. Heinz, H. Song, and A. K. Chaudhuri, Phys. Rev. C **73**, 034904 (2006).
[38] R. Baier, P. Romatschke, and U. A. Wiedemann, Phys. Rev. C **73**, 064903 (2006).
[39] T. Koide, G. S. Denicol, Ph. Mota, and T. Kodama, Phys. Rev. C **75**, 034909 (2007).
[40] R. Baier, P. Romatschke, D. T. Son, A. O. Starinets, and M. A. Stephanov, J. High Energy Phys. 04 (2008) 100.
[41] J. M. Maldacena, Adv. Theor. Math. Phys. **2**, 231 (1998); Int. J. Theor. Phys. **38**, 1113 (1999).
[42] S. Bhattacharyya, V. E. Hubeny, S. Minwalla, and M. Rangamani, J. High Energy Phys. 02 (2008) 045.
[43] D. Kharzeev and K. Tuchin, arXiv:0705.4280 [hep-ph].
[44] S. Sakai and A. Nakamura, POS LAT **2007**, 221 (2007).
[45] H. B. Meyer, Phys. Rev. Lett. **100**, 162001 (2008).
[46] F. Karsch, D. Kharzeev, and K. Tuchin, Phys. Lett. **B663**, 217 (2008).
[47] A. Muronga, Phys. Rev. Lett. **88**, 062302 (2002); **89**, 159901(E) (2002).
[48] M. Natsuume and T. Okamura, Phys. Rev. D **77**, 066014 (2008).
[49] R. Baier and P. Romatschke, Eur. Phys. J. C **51**, 677 (2007).
[50] P. Huovinen and P. V. Ruuskanen, Annu. Rev. Nucl. Part. Sci. **56**, 163 (2006).
[51] C++ versions of the relativistic viscous hydrodynamic codes with and without radial symmetry may be obtained from http://hep.itp.tuwien.ac.at/~paulrom/.

[52] *Numerical Recipes in C,* 2nd ed. (Cambridge University, Cambridge, England, 1992).
[53] A. Dumitru, E. Molnar, and Y. Nara, Phys. Rev. C **76**, 024910 (2007).
[54] Y. Aoki, G. Endrodi, Z. Fodor, S. D. Katz, and K. K. Szabo, Nature (London) **443**, 675 (2006).
[55] M. Laine and Y. Schroder, Phys. Rev. D **73**, 085009 (2006).
[56] C. M. Hung and E. V. Shuryak, Phys. Rev. C **57**, 1891 (1998).
[57] F. Cooper and G. Frye, Phys. Rev. D **10**, 186 (1974).
[58] P. V. Ruuskanen, Acta Phys. Pol. B **18**, 551 (1987).
[59] D. H. Rischke and M. Gyulassy, Nucl. Phys. **A608**, 479 (1996).
[60] S. R. de Groot, W. A. van Leeuwen, and C. G. van Weert, *Relativistic Kinetic Theory* (North-Holland, Amsterdam, 1980).
[61] P. F. Kolb and U. W. Heinz, in *Quark-Gluon Plasma 3*, edited by R. C. Hwa and X.-N. Wang (World Scientific, Singapore, 2004).
[62] J. Sollfrank, P. Koch, and U. W. Heinz, Phys. Lett. **B252**, 256 (1990).
[63] J. Sollfrank, P. Koch, and U. W. Heinz, Z. Phys. C **52**, 593 (1991).
[64] AZHYDRO Version 0.2, available from http://karman.physics.purdue.edu/OSCAR.
[65] S. A. Bass and A. Dumitru, Phys. Rev. C **61**, 064909 (2000).
[66] D. Teaney, J. Lauret, and E. V. Shuryak, arXiv:nucl-th/0110037.
[67] T. Hirano, U. W. Heinz, D. Kharzeev, R. Lacey, and Y. Nara, Phys. Lett. **B636**, 299 (2006).
[68] C. Nonaka and S. A. Bass, Phys. Rev. C **75**, 014902 (2007).
[69] R. S. Bhalerao and S. Gupta, Phys. Rev. C **77**, 014902 (2008).
[70] G. Baym, B. L. Friman, J. P. Blaizot, M. Soyeur, and W. Czyz, Nucl. Phys. **A407**, 541 (1983).
[71] M. Chojnacki and W. Florkowski, Phys. Rev. C **74**, 034905 (2006).
[72] M. I. Nagy, T. Csorgo, and M. Csanad, Phys. Rev. C **77**, 024908 (2008).
[73] D. Kharzeev, E. Levin, and M. Nardi, Nucl. Phys. **A730**, 448 (2004); **A743**, 329(E) (2004).
[74] A. Adil, H. J. Drescher, A. Dumitru, A. Hayashigaki, and Y. Nara, Phys. Rev. C **74**, 044905 (2006).
[75] L. D. McLerran and R. Venugopalan, Phys. Rev. D **49**, 2233 (1994).
[76] L. D. McLerran and R. Venugopalan, Phys. Rev. D **49**, 3352 (1994).
[77] T. Lappi and R. Venugopalan, Phys. Rev. C **74**, 054905 (2006).
[78] P. F. Kolb, J. Sollfrank, and U. W. Heinz, Phys. Lett. **B459**, 667 (1999).
[79] J. Y. Ollitrault, Phys. Rev. D **46**, 229 (1992).
[80] P. F. Kolb, J. Sollfrank, and U. W. Heinz, Phys. Rev. C **62**, 054909 (2000).
[81] U. W. Heinz, AIP Conf. Proc. **739**, 163 (2005).
[82] M. Lublinsky and E. Shuryak, Phys. Rev. C **76**, 021901(R) (2007).
[83] S. S. Adler *et al.* (PHENIX Collaboration), Phys. Rev. C **69**, 034909 (2004).
[84] B. Alver *et al.* (PHOBOS Collaboration), Int. J. Mod. Phys. E **16**, 3331 (2008).
[85] J. Y. Ollitrault, Nucl. Phys. **A590**, 561C (1995).
[86] B. I. Abelev *et al.* (STAR Collaboration), Phys. Rev. C **77**, 054901 (2008).
[87] A. Poskanzer (private communication).
[88] P. K. Kovtun, D. T. Son, and A. O. Starinets, Phys. Rev. Lett. **94**, 111601 (2005).
[89] P. Huovinen, talk given at RHIC Winter Workshop, INT, Seattle, 2002 (unpublished).
[90] W. Broniowski, M. Chojnacki, W. Florkowski, and A. Kisiel, Phys. Rev. Lett. **101**, 022301 (2008).
[91] T. Hirano and M. Gyulassy, Nucl. Phys. **A769**, 71 (2006).
[92] T. Schafer, Phys. Rev. A **76**, 063618 (2007).
[93] S. Gavin and M. Abdel-Aziz, Phys. Rev. Lett. **97**, 162302 (2006).
[94] A. Adare *et al.* (PHENIX Collaboration), Phys. Rev. Lett. **98**, 172301 (2007).
[95] H. J. Drescher, A. Dumitru, C. Gombeaud, and J. Y. Ollitrault, Phys. Rev. C **76**, 024905 (2007).
[96] J. Adams *et al.* (STAR Collaboration), J. Phys. G **32**, L37 (2006).
[97] P. Sorensen (STAR Collaboration), J. Phys. G **34**, S897 (2007).
[98] S. Vogel, G. Torrieri, and M. Bleicher, arXiv:nucl-th/0703031.
[99] H. J. Drescher and Y. Nara, Phys. Rev. C **76**, 041903(R) (2007).
[100] T. A. Trainor, Mod. Phys. Lett. A **23**, 569 (2008).
[101] Y. Hama, R. Peterson, G. Andrade, F. Grassi, W. L. Qian, T. Osada, C. E. Aguiar, and T. Kodama, arXiv:0711.4544 [hep-ph].
[102] P. Romatschke, arXiv:0710.0016 [nucl-th].